COUNTERFACTUAL GENERATIVE MODELING WITH VARIATIONAL CAUSAL INFERENCE

Anonymous authors
Paper under double-blind review

ABSTRACT

Estimating an individual's potential outcomes under counterfactual treatments is a challenging task for traditional causal inference and supervised learning approaches when the outcome is high-dimensional (e.g. gene expressions, facial images) and covariates are relatively limited. In this case, to predict one's outcomes under counterfactual treatments, it is crucial to leverage individual information contained in its high-dimensional observed outcome in addition to the covariates. Prior works using variational inference in counterfactual generative modeling have been focusing on neural adaptations and model variants within the conditional variational autoencoder formulation, which we argue is fundamentally ill-suited to the notion of counterfactual in causal inference. In this work, we present a novel variational Bayesian causal inference framework and its theoretical backings to properly handle counterfactual generative modeling tasks, through which we are able to conduct counterfactual supervision end-to-end during training without any counterfactual samples, and encourage disentangled exogenous noise abduction that aids the correct identification of causal effect in counterfactual generations. In experiments, we demonstrate the advantage of our framework compared to state-of-the-art models in counterfactual generative modeling on multiple benchmarks.

1 INTRODUCTION

In traditional causal inference, heterogeneous treatment effect is typically formulated as the intervention model $p(Y|X, \mathrm{do}(T))$ (or $\mathbb{E}[Y|X, \mathrm{do}(T)]$) with outcome Y, covariates X, treatment T, and estimated by the observed covariate-specific efficacy $p(Y|X, T)$ under the ignorability assumption (Rosenbaum & Rubin, 1983; Pearl, 1995) using various supervised learning and estimation techniques. However, in cases such as the single-cell perturbation datasets (Dixit et al., 2016; Norman et al., 2019; Schmidt et al., 2022) where Y has thousands of dimensions while X has two or three categorical features, such model could hardly be relied on to produce useful individualized results. To construct outcome Y' under a counterfactual treatment T' in such high-dimensional outcome scenario, it is important and necessary to learn the individual-specific efficacy $p(Y'|Y, X, T, T')$ conditioning on the factual outcome Y itself, which leverages the rich information embedded in the factual outcome that cannot be recovered by the handful of covariates. For example, given a cell with type A549 (X) that received SAHA drug treatment (T), we may want to know what its gene expression profile (Y') would look like if it had received Dex drug treatment (T') instead. In this case, we would want to take the profiles of other cells with type A549 that indeed received Dex as reference, such that the counterfactual construction Y' exhibits the treatment characteristics of Dex on A549, but would also want to extract as much individual information as possible from its own expression profile (Y) such that the counterfactual construction could preserve this cell's individuality.

Yet the lack of observability of counterfactual outcome Y' makes this objective intractable and hence presents a major difficulty for supervised learning when Y is taken as an input. In previous works that involve self-supervised counterfactual generation (Kocaoglu et al., 2017; Louizos et al., 2017; Yoon et al., 2018; Pawlowski et al., 2020; Yang et al., 2021; Kim et al., 2021; Lotfollahi et al., 2021; Sauer & Geiger, 2021; Feng et al., 2022; Shen et al., 2022) based on Variational Autoencoders (VAE) (Kingma & Welling, 2013) and Generative Adversarial Networks (GAN) (Goodfellow et al., 2014), there is no counterfactual supervision during training, and hence no explicit regulation on the trade-off between treatment characteristics and individuality. When such regulation does not exist, there is a disconnection between training and counterfactual inference. To see this, consider a conditional

generative model $g_\theta(y, t)$ that is only supervised on the reconstruction loss with respect to outcome y during training. In this case, the model is free to ignore the extra treatment t and converge to a state such that $g_\theta(y, t) = g_\theta(y, 0)$ (Chen et al., 2016), hence preserving maximum individuality yet minimum treatment characteristics in counterfactual construction $g_\theta(y, t')$ during inference. This is particularly an issue for high-fidelity counterfactual generation with state-of-the-art Hierarchical Variational Autoencoders (HVAE) (Vahdat & Kautz, 2020; Child, 2020), as the latent representations possess even larger number of bottleneck dimensions compared to the observed outcome y. In more recent works on counterfactual generative modeling with HVAEs and diffusion models (Sanchez & Tsaftaris, 2022; Monteiro et al., 2023; Ribeiro et al., 2023), only Ribeiro et al. (2023) touched on the issue of counterfactual supervision, yet its proposed method does not have a theoretical backing in variational inference, nor could it be conducted end-to-end during training. As we will see in the proceeding sections of this work, there is a fundamental incompatibility of the conditional VAE formulation with counterfactual generative modeling, which is the root cause of such issue. In fact, this incompatibility also exhibits itself in another important aspect of counterfactual generative modeling which is latent disentanglement – the partially abducted exogenous noise (i.e. shallow-level latent representation) in conditional HVAEs and diffusion models is able to encode individuality better than traditional VAEs, but at the same time is still heavily entangled with treatment variables and often result in lingering characteristics of the factual treatment in counterfactual construction (Monteiro et al., 2023; Sanchez & Tsaftaris, 2022). More introduction regarding latent disentanglement can be found in Appendix A.

Our contributions in this work are summarized as follow: **1)** we propose a formulation and stochastic optimization scheme for counterfactual generative modeling by specifically formulating counterfactual variables and using variational inference to derive the evidence lower bound (ELBO) for the individual-level likelihood $p(Y'|Y, X, T, T')$ – a well-motivated and fitting objective for counterfactual generative modeling instead of the marginal-level (interventional) conditional likelihood $p(Y|X, T)$ or even joint likelihood $p(Y, X, T)$ used by VAE-based prior works. **To emphasize, the contribution here is not to propose another model variant under the conditional VAE formulation such as HVAEs or diffusion models (Sanchez & Tsaftaris, 2022; Monteiro et al., 2023; Ribeiro et al., 2023), but to fundamentally change the VAE formulation.** We call this framework Variational Causal Inference (VCI). An explanation to why the conditional VAE formulation (including diffusion models) is ill-suited to counterfactual generative modeling and a straightforward comparison between VAE's formulation and ours can be found in Appendix B. **2)** Our proposed optimization scheme allows us to conduct **counterfactual supervision end-to-end during training** alongside self-supervision, even without any counterfactual observations, which has not been done in prior works to the best of our knowledge. **3)** This workflow of constructing and supervising counterfactual outcomes during training presents us the unique opportunity to naturally enforce **disentangled exogenous noise abduction through distribution alignment** on matching pairs (Shu et al., 2019; Locatello et al., 2020; Brehmer et al., 2022) without having paired data, which has not been done in counterfactual generative modeling, to the best of our knowledge. **4)** We further propose a robust estimation scheme for high-dimensional marginal causal parameters leveraging this individual-level counterfactual construction framework. No prior work in counterfactual generative modeling conducts such asymptotically efficient marginal estimation upon acquiring individual predictions, to the best of our knowledge. **5)** In experiments, our proposed method is evaluated on datasets with vector outcomes – single cell perturbation datasets, as well as datasets with image outcomes – facial imaging and handwritten digits datasets, and compared to state-of-the-art models in the two domains. The results show that ours outperformed state-of-the-arts in both domains with notable margins. **Related work and comparative analysis can be found in Appendix C.**

2 Proposed Method

2.1 Formulations and Intuitions

Let outcome Y be a random vector, X be a mix of categorical and real-valued covariates, T be a categorical or real-valued treatment (or multiple treatments) and Z be a real-valued latent feature vector. Suppose the causal relations between random variables (and random vectors) follow a structural causal model (SCM) (Pearl, 1995) defined in Figure 1, where we adopt twin networks (Balke & Pearl, 1994) to formulate counterfactuals Y' and T' as separate variables apart from Y and T having a conditional distribution $p(Y', T'|Z, X)$ identical to that of its factual counterpart

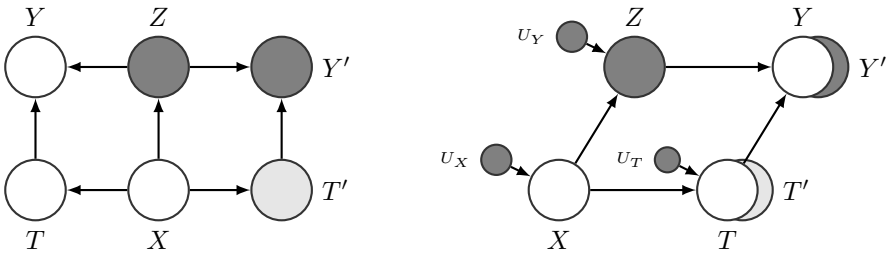

(a) Bayesian network (b) Counterfactual view of the Bayesian network

Figure 1: The causal diagram where variables are generated from the following SCM: $X = f_X(U_X)$; $T = f_T(X, U_T)$, $T' = f_T(X, U'_T)$ where U_T, U'_T are i.i.d.; $Z = f_Z(X, U_Y)$; $Y = f_Y(Z, T, \epsilon_Y)$, $Y' = f_Y(Z, T', \epsilon'_Y)$ where ϵ_Y, ϵ'_Y are i.i.d., independent of all Us, and are constants w.p. 1 if the consistency assumption is assumed. Endogenous variables follow the Bayesian network on the left under the ignorability assumption, with permissibly one additional edge from either Z or T to X if U_Y or U_T is dependent of U_X. We call $O = (X, T, Y)$ observed variables, $B = (X, T, T', Y)$ sample variables (T' are sampled for model training and evaluation), $D = (X, T, T', Y, Y')$ full data variables and $W = (Z, X, T, T', Y, Y')$ all variables. White nodes are observed, light grey nodes are assigned during training and inference, dark grey nodes are unobserved.

$p(Y, T|Z, X)$. Different from Vlontzos et al. (2023), we introduce latent Z in high-dimensional outcome settings as a feature vector of Y such that random factor ϵ_Y does not capture any more uncertainty that can be retrieved from its counterfactual counterpart, i.e. $\epsilon_Y \perp\!\!\!\perp Y'$ and similarly $\epsilon'_Y \perp\!\!\!\perp Y$. The consistency and ignorability assumptions corresponding to this new causal formulation can be found in Appendix H. Under the consistency assumption (Assumption 2 and Remark 2), $\epsilon_Y = 0$ and there is no more uncertainty in Y beyond Z, i.e. the shared random factor U_Y fully captures the exogenous noise injected to Y and Y'. Hence, Z in this setting can be seen as an unobserved summary random vector of the covariates X and exogenous noise U_Y. Note that the consistency assumption is not generally required for our subsequent variational inference, but is required for $Y'_{\text{do}(T')}$ to be formally defined as the counterfactual of Y under the three layer causal hierarchy of Pearl (2009). The ignorability assumption (Assumption 1 and Remark 1) is generally required, under which $do(T' = t')$ and $T' = t'$ result in the same outcome distribution on Y' conditioned on X or Z. See Appendix D for the connection between our formulation and the traditional SCM formulation.

Under this formulation, Z has a posterior distribution $p(Z|Y, T, X)$ given the observed variables; Y and Y' can be constructed by $p(Y|Z, T)$ and $p(Y'|Z, T')$ respectively with latent features Z. Similar to prior works in autoencoder (Vincent et al., 2008; Bengio et al., 2014), we estimate the latent recognition model (i.e. exogenous noise abduction model) and outcome construction model with deep neural network encoder q_ϕ and decoder p_θ. Given a sample $b = (x, t, t', y)$, while the reconstruction $y_{\theta,\phi}$ of y is self-supervised, we can only assess the counterfactual construction $y'_{\theta,\phi}$ under t' by looking at its resemblance to similar individuals that indeed received treatment t'. Hence, naively, we may conduct counterfactual supervision during training with a semi-autoencoding (SAE) loss function as follow

$$L_{\theta,\phi}(b) = L_2(y_{\theta,\phi}, y) - \omega \cdot \ell_{\hat{p}(Y'|x,t')}(y'_{\theta,\phi}) \tag{1}$$

where ω is a scaling coefficient and $\hat{p}$ is the traditional covariate-specific outcome model fit on the observed variables (X, T, Y) (notice that $p(Y'|x, T' = t') = p(Y|x, T = t')$). The intuition is that, if $y'_{\theta,\phi}$ is indeed one's outcome under t', then the likelihood of $y'_{\theta,\phi}$ coming from the outcome distribution of individuals with the same attributes x that factually received treatment t' should be high. In practice, we can fit $\hat{p}(Y|X, T)$ in an end-to-end fashion using a discriminator $\mathcal{D}(X, T, Y)$ on factual triplets (x, t, y) and counterfactual triplets $(x, t', y'_{\theta,\phi})$ with the adversarial approach (Goodfellow et al., 2014). Specifically, we use discriminator loss $L_{\mathcal{D}}(b, y'_{\theta,\phi}) = -\log[\mathcal{D}(x, t, y)] - \log[1 - \mathcal{D}(x, t', y'_{\theta,\phi})]$ to train model $\mathcal{D}$, and use generator loss $\ell_{\hat{p}(Y'|x,t')}(y'_{\theta,\phi}) = \log \mathcal{D}(x, t', y'_{\theta,\phi})$ in $L_{\theta,\phi}(b)$ (notice that $p(X, T) = p(X, T')$). This end-to-end approach prevents (p_θ, q_ϕ) from exploiting a pre-trained $\hat{p}$ model. The SAE trained through the adversarial approach motivates the derivation of our main theorem presented in the next section, and serves as a baseline comparison

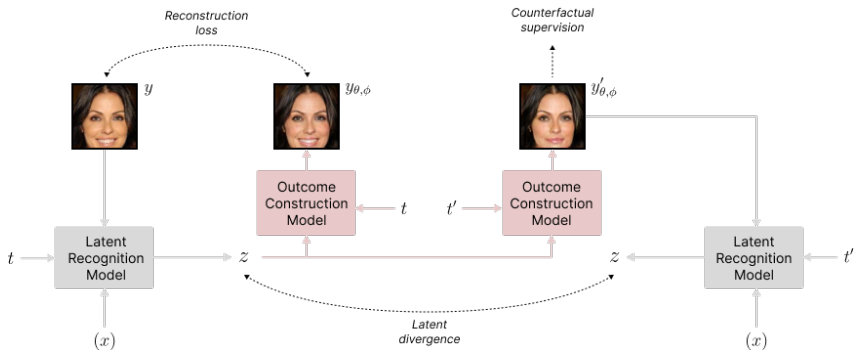

Figure 2: Model workflow of the Variational Causal Inference (VCI) framework. In a forward pass, the encoding model takes outcome y as well as its treatments t and covariates x (if any) as inputs and attains latent feature z; (z, t) and (z, t') where t' is the counterfactual treatments are separately passed into the decoding model to attain reconstruction $y_{\theta,\phi}$ and counterfactual construction $y'_{\theta,\phi}$, for which reconstruction loss and counterfactual supervision loss are evaluated; $y'_{\theta,\phi}$ is then passed back into the encoding model along with t' and x to attain z again, which is encouraged to match the latent feature z previously acquired from encoding the factual outcome y and treatment t through the latent divergence term. The neural architectures of the latent recognition and outcome construction models for image generation tasks can be found in Appendix J.

to our main algorithm in the ablation study of the experiments section. In cases where covariates are limited and discrete such as the single-cell perturbation datasets, $\hat{p}(Y|X,T)$ can simply be a smoothed empirical outcome distribution under treatment T stratified by covariates X.

2.2 Variational Causal Inference

Now we present our main result by rigorously formulating the objective, providing a probabilistic theoretical backing, and specifying an optimization scheme that reflects the intuition described in the previous section. Suppose we want to optimize $p(Y'|Y,X,T,T')$ instead of the traditional outcome likelihood $p(Y|X,T)$. The following theorem induces the evidence lower bound (ELBO) and thus provides a roadmap for stochastic optimization:

Theorem 1. *Suppose a collection of random variables W follows a causal structure defined by the Bayesian network in Figure 1. Then $J(D) = \log[p(Y'|Y,X,T,T')]$ has the following variational lower bound:*

$$\begin{aligned} J(D) \geq \mathbb{E}_{p(Z|Y,T,X)} \log\left[p(Y|Z,T)\right] - D\left[p(Y|X,T) \parallel p(Y'|X,T')\right] \\ - D_{\mathrm{KL}}\left[p(Z|Y,T,X) \parallel p(Z|Y',T',X)\right] \end{aligned} \tag{2}$$

where $D[p \parallel q] = \log p - \log q$.

Proof of Theorem 1 and proofs of all theoretical results in the following sections can be found in Appendix I. Theorem 1 suggests that, in order to maximize the individual-specific outcome likelihood $p(Y'|Y,X,T,T')$, we can instead maximize the following estimated ELBO parameterized with estimating models p_θ and q_ϕ:

$$\begin{aligned} J_{\theta,\phi}(b) = \mathbb{E}_{q_\phi(z|y,t,x)} \log\left[p_\theta(y|z,t)\right] + \log\left[\hat{p}(y'_{\theta,\phi}|x,t')\right] \\ - D_{\mathrm{KL}}\left[q_\phi(Z|y,t,x) \parallel q_\phi(Z|y'_{\theta,\phi},t',x)\right], \end{aligned} \tag{3}$$

where $y'_{\theta,\phi} = \mathbb{E}_{p_\theta(Y'|\mathbb{E}_{q_\phi(Z|y,t,x)}Z,t')}Y'$ and $\hat{p}$ can be estimated with the approaches described at the end of Section 2.1. Note that $\hat{p}(y|x,t)$ does not impose gradient on (p_θ, q_ϕ) and is thus omitted in $J_{\theta,\phi}(b)$. The stochastic optimization of ELBO is hence conducted on the objective $J_{p_{\mathrm{data}}}(p_\theta, q_\phi) = \mathbb{E}_{p_{\mathrm{data}}} J_{\theta,\phi}(b)$ where $t' \sim p_{\mathrm{data}}(T|x)$. A figure demonstrating the workflow of this stochastic optimization scheme can be found in Figure 2.

As can be seen, Equation 3 consists of the expected individual-specific reconstruction likelihood $E_{q_\phi(z|y,t,x)} \log[p_\theta(Y|z,t)]$ and the covariate-specific counterfactual outcome likelihood

$\log[p(y'_{\theta,\phi}|x,t')]$, echoing the intuition highlighted by Equation 1, with an additional divergence term $-D_{\mathrm{KL}}[q_\phi(Z|y,t,x) \parallel q_\phi(Z|y'_{\theta,\phi},t',x)]$ that regularizes the similarity across latent distributions under different potential scenarios. Note that this framework is fundamentally different from any VAE based formulation such as CVAE (Sohn et al., 2015) or CEVAE (Louizos et al., 2017) (note that they work towards conditional generations and heterogeneous treatment effects), since the variational lower bound is derived directly from the causal objective and the KL-divergence term serves causal purposes that are entirely different from the prior latent bounding purpose of VAEs. An explanation of this divergence term is given in the paragraph below. A comparison between VCI and conditional VAE using standard VAE notations is given in Appendix B. A summary of different optional gradient detaching patterns for training stability is given in Appendix K. An approach to conduct counterfactual supervision implicitly using traditional variational inference is given in Appendix E.

Divergence Interpretation The divergence term $-D_{\mathrm{KL}}[q_\phi(Z|y,t,x) \parallel q_\phi(Z|y'_{\theta,\phi},t',x)]$ is the key of the framework and it serves two purposes. Firstly, it adds robustness to latent encoding by encouraging the encoding model to recognize individual features contained in both factual and counterfactual outcomes. In fact, these common features are well disentangled from the treatment variables, which we will discuss in-depth in the next section. Secondly, it encourages the preservation of individuality in counterfactual outcome constructions. To see this, notice that if the counterfactual outcome construction was only penalized by the covariate-specific likelihood loss $-\log[\hat{p}(y'_{\theta,\phi}|x,t')]$, the counterfactual decoding model $p_\theta(Y'|z_\phi,t')$ could learn to completely discard the identity of individual subjects represented in latent features z_ϕ once it detects a counterfactual treatment $t' \neq t$ in the inputs. Such behavior is regulated by the divergence term, since otherwise we would not be able to recover a latent distribution $q_\phi(Z|y'_{\theta,\phi},t',x)$ close to $q_\phi(Z|y,t,x)$.

Robust Marginal Estimation Similar to the augmented inverse propensity weighted (AIPW) estimator in traditional causal inference, the individual-level model predictions acquired by our framework can also aid the robust estimation of average treatment effect $\Psi(p) = \mathbb{E}_p[Y'_{\mathrm{do}(T'=\alpha)}]$ for a treatment level α of interest if such estimation is desired. Under the formulation in Figure 1, we have the following robust estimator that is asymptotically efficient under some regularity conditions (Van Der Laan & Rubin, 2006):

$$\hat{\Psi}_n(o) = \frac{1}{n}\sum_{k=1}^{n}\left\{\frac{I(t_k=\alpha)}{\hat{e}(t_k|x_k)}\cdot y_k + \left(1-\frac{I(t_k=\alpha)}{\hat{e}(t_k|x_k)}\right)\cdot \mathbb{E}_{p_\theta}\left[Y'|z_{k,\phi},T'=\alpha\right]\right\}, \tag{4}$$

where $o_k = (x_k,t_k,y_k) \overset{\text{iid}}{\sim} p(x,t,y)$ is the vector of observed triplet of the k-th individual, $z_{k,\phi} \sim q_\phi(y_k,t_k,x_k)$, and $\hat{e}$ is an estimation of the propensity score that satisfies the positivity assumption (Robins, 1986). See Appendix G for the derivation of this estimator. Notice that the regression adjustment term $\mathbb{E}_{p_\theta}[Y'|z_{k,\phi},T'=\alpha]$ in ours has the ability to vary across different individuals within the same covariate group (which is not the case for that of the AIPW estimator in traditional causal formulation) and it is meaningful to conduct the robust estimation of covariate-specific marginal treatment effect $\Xi(p) = \mathbb{E}_p[Y'_{\mathrm{do}(X=c,T'=\alpha)}]$ for a given covariate c of interest, see Appendix G for details.

2.3 Latent Identifiability and Exogenous Noise Disentanglement

In any deep probabilistic model, there is a certain degree of freedom and arbitrarity to the learnt latent distribution, even with latent restrictions. Naturally, one might question the latent identification of our variational causal framework: when identifying counterfactual Y' under T', does the learnt latent Z inevitably carry over some characteristics of the factual treatment in Y and T? Ideally, we would like to aid counterfactual construction by attaining a clean disentanglement between the learnt latent and the observed treatment, such that the counterfactual generation does not preserve influence from the factual treatment. Such disentangled exogenous noise abduction fits the semantic of our generating process (Figure 1), where Z and T are not descendant of each other and $Z \perp\!\!\!\perp T|X$, as well as the semantic of causal identification in the traditional formulation, where the identifiability of $Y_{\mathrm{do}(T)}$ relies on the ignorability assumption that exogenous noise does not contain unobserved confounders. In this section, we show that optimizing the VCI framework in fact grants such disentanglement between Z and T under mild assumptions, leading to a more in-depth understanding of the purpose and behavior of the latent divergence term in VCI's optimization scheme.

Similar to Shu et al. (2019), we formally define and measure disentanglement in terms of (encoder) consistence and (encoder) restrictiveness, except that our definitions are generalized to the case of stochastic models and models with auxiliary attributes. For notation simplicity of the oracle operation on functions with auxiliary inputs, we use $\gamma \circ \zeta(a; b)$ to denote $\gamma(c, b)$ where $c = \zeta(a)$ if ζ is a deterministic function and $c \sim \zeta(a)$ if ζ is a probability measure. The definitions of consistence, restrictiveness, and disentanglement are then given in Appendix F.

Consider our model class $\{(p_\cdot, q_\cdot) \mid p_\cdot : \mathcal{Z} \times \mathcal{T} \to [0,1]^{\Sigma_\mathcal{Y}},\ q_\cdot : \mathcal{Y} \times \mathcal{T} \times \mathcal{X} \to [0,1]^{\Sigma_\mathcal{Z}}\}$ and let $S := (Z, T)$, $V := (Y, T)$. We regard T as part of the model outputs such that the oracle operations above are well-defined, i.e. let $\mathcal{H} = \{(\tilde{p}_\cdot, \tilde{q}_\cdot) \mid \tilde{p}_\cdot(s) = p_\cdot(Y|z,t) \times \delta_t(T),\ \tilde{q}_\cdot(v, x) = q_\cdot(Z|y,t,x) \times \delta_t(T)\}$ where δ_t is the Dirac measure ($\delta_t(T) = 1$ if $T = t$ else 0). Then we have the following lemma:

Lemma 1. *If q minimizes latent divergence in Equation 2 over $p_0(D)$, i.e.*

$$\mathbb{E}_{p_0} D_{\mathrm{KL}} \left[q(Z|y,t,x) \parallel q(Z|y',t',x) \right] = 0, \tag{5}$$

then $\tilde{q}$ disentangles Z and T.

Lemma 1 builds a direct connection between the latent divergence term and the disentangled abduction of exogenous noise. Intuitively, it states that if the encoder encodes the same latent representation for any pair of potential outcomes of the same individual, then the latent representation must have been disentangled from the treatment. However, does optimizing the ELBO necessarily imply that the latent divergence term reaches the minimum? We proceed to show that this is indeed implied under mild assumptions.

Proposition 1. *With the true distribution p_0 satisfying Assumption 2 and Assumption 3, if (p_*, q_*) maximizes the evidence lower bound over $p_0(D)$ and any $\hat{p}$, i.e.*

$$\begin{aligned}(p_*, q_*) \in \arg\max_{p_\cdot, q_\cdot} \mathbb{E}_{p_0} \big\{ & \mathbb{E}_{q_\cdot(z|y,t,x)} \log \left[p_\cdot(y|z,t) \right] + \log \left[\hat{p}(y'|x,t') \right] \\ & - D_{\mathrm{KL}} \left[q_\cdot(Z|y,t,x) \parallel q_\cdot(Z|y',t',x) \right] \big\}\end{aligned} \tag{6}$$

then $\tilde{q}_*$ disentangles Z and T.

Intuitively, Proposition 1 states that as long as the treatments do not have any unknown side effect and do not completely wipe out different features in different individuals, the solution to maximizing the ELBO disentangles Z and T. In practice, we formulate model class as deterministic functions (i.e. degenerate distributions) plus noise similar to prior work, and encoder noise as standard normal:

$$\left\{ p_\cdot \mid g_\cdot(Y|z,t) := \delta_{\mathbb{E}_{p_\cdot(Y|z,t)} Y},\ \epsilon_\cdot(z,t) := p_\cdot(Y - \mathbb{E}_{p_\cdot(Y|z,t)} Y | z, t) \right\} \tag{7}$$

$$\left\{ q_\cdot \mid e_\cdot(Z|y,t,x) := \delta_{\mathbb{E}_{q_\cdot(Z|y,t,x)} Z},\ q_\cdot(Z - \mathbb{E}_{q_\cdot(Z|y,t,x)} Z | y, t, x) = \mathcal{N}(0,1) \right\} \tag{8}$$

and learn model $e_\cdot$, $g_\cdot$ and $\epsilon_\cdot$ during training. The following proposition states that disentanglement under the estimating model's own oracle can be achieved by optimizing the VCI objective in real-world optimizations, where neither the true generating mechanisms nor the true factual-counterfactual pairs are available.

Proposition 2. *Given dataset $\{(x_k, t_k, y_k)\}|_{k=1}^n$, let p_{data} be its empirical distribution and the model class in Equation 7 and Equation 8 satisfy the following uniqueness conditions:*

1) *$\forall \alpha \in \mathcal{T}$, we have $g_\cdot(Y|z,\alpha) \neq g_\cdot(Y|z',\alpha)$ if $z \neq z'$;*
2) *$\forall x, t, y, t' : p_{\mathrm{data}}(x,t,y) \cdot p_{\mathrm{data}}(t'|x) > 0$ and $y'_\cdot = \mathbb{E}_{g_\cdot(Y|z,t') e_\cdot(z|y,t,x)} Y$, we have $p_{\mathrm{data}}(x, t', y'_\cdot) = 0$ if $(x,t,y) \neq (x,t',y'_\cdot)$.*

If (p_*, q_*) maximizes the VCI objective in Equation 3 over p_{data} and any $\hat{p}$, i.e.

$$(p_*, q_*) \in \arg\max_{p_\cdot, q_\cdot} J_{p_{\mathrm{data}}}(p_\cdot, q_\cdot) \tag{9}$$

then $(\tilde{g}_*, \tilde{q}_*)$ disentangles Z and T under $\int_y e_* p_{\mathrm{data}}$.

We note that uniqueness condition 2) in Proposition 2 is completely reasonable in high-dimensional outcome settings: taking the facial imaging dataset as an example, it wouldn't make any sense for a model's constructed image for a certain individual to be an exact match of the factual outcome of another individual in the dataset, as long as the dataset does not contain multiple images of the same individual under the same setting.

Corollary 1. *Under the same settings and conditions of Proposition 2,* $(\tilde{g}_*, \tilde{e}_*)$ *disentangles* Z *and* T *under* $\int_y e_* p_{\text{data}}$.

Corollary 1 states that the optimal model is guaranteed to disentangle Z and T under the constructed latent distribution in inference mode without noise injection. In summary, the disentanglement results in our framework rely on the simple fact that the latent divergence term is established on an individual level, and does not necessarily compete with outcome supervisions under mild assumptions. Prior works in VAEs have proposed bounding latent on conditional marginal prior (Sohn et al., 2015; Khemakhem et al., 2020), and VCI can be seen as a further relaxed form of latent restriction in the sense that the latent for any given subject need not be restricted to any prior distribution – we only require the latent distributions of a subject's different potential outcomes to match each other. More insights on how the latent divergence term helps the training of VCI in practice can be found in the ablation study in the experiments section.

3 EXPERIMENTS

We present experimental results of our framework on two datasets with vector outcomes (sci-Plex dataset from Srivatsan et al. (2020) (Sciplex) and the CRISPRa dataset from Schmidt et al. (2022) (Marson)) and two datasets with image outcomes: Morpho-MNIST (Castro et al., 2019) and CelebA-HQ (Karras et al., 2017). Results from the former are compared to state-of-the-art models in single-cell perturbation prediction and results from the latter are compared to state-of-the-art models in counterfactual image generation. In both cases, our model exhibited superior performance against benchmarks. Details of model and dataset settings for each experiment can be found in Appendix O.

3.1 SINGLE-CELL PERTURBATION DATASETS

Same as Lotfollahi et al. (2021), we evaluate our model and benchmarks on a widely accepted and biologically meaningful metric — the R^2 (coefficient of determination) of the average prediction against the true average from the out-of-distribution (OOD) set on all genes and differentially-expressed (DE) genes. Definitions of OOD set and DE genes can be found in Appendix O.1. Results over five independent runs are shown in Table 1.

Table 1: $\bar{R^2}$ of OOD predictions on single-cell perturbation datasets. AE is a naive baseline adapting Autoencoder to counterfactual generation, see Appendix L.1. GANITE is GANITE's counterfactual block adapting to high-dimensional outcome plus multi-level treatment (see Appendix L.2).

	Sciplex		Marson	
	all genes	DE genes	all genes	DE genes
AE	0.740 ± 0.043	0.421 ± 0.021	0.804 ± 0.020	0.448 ± 0.009
CEVAE (Louizos et al., 2017)	0.760 ± 0.019	0.436 ± 0.014	0.795 ± 0.014	0.424 ± 0.015
GANITE (Yoon et al., 2018)	0.751 ± 0.013	0.417 ± 0.014	0.795 ± 0.017	0.443 ± 0.025
CPA (Lotfollahi et al., 2021)	$\mathbf{0.836} \pm 0.002$	0.474 ± 0.014	0.876 ± 0.005	0.549 ± 0.019
VCI	0.832 ± 0.008	$\mathbf{0.496} \pm 0.011$	$\mathbf{0.891} \pm 0.007$	$\mathbf{0.658} \pm 0.040$

For each perturbation of each covariate level (e.g. each cell type of each donor) in the OOD set, the R^2 (coefficient of determination) is computed with the average outcome predictions for all genes and DE genes using samples from the validation set against the true empirical average over samples from the OOD set. The average R^2 over all perturbations of all covariate levels is then calculated as the evaluation metric $\bar{R^2}$. In these experiments, our variational Bayesian causal inference framework excelled state-of-the-art models in both experiments, with the largest fractional improvement on DE genes which are most causally affected by the perturbations. **Results of marginal estimation using the robust estimator can be found in Appendix P.1.**

3.2 MORPHO-MNIST

In an ideal world, we would like to evaluate model performance against benchmarks simply by measuring the mean squared error (MSE) between counterfactual construction and the counterfactual

Table 2: The MSE of the counterfactual image and the MAE of its thickness and intensity against the counterfactual truth on Morpho-MNIST. Our model is evaluated against the state-of-the-art model in adversarial formulation DEAR (Shen et al., 2022) and state-of-the-arts in variational formulation CHVAE (Monteiro et al., 2023), MED (Ribeiro et al., 2023). Images are scaled to $[0, 1]$ in evaluations. Note that our test set is constructed to be much harder than that of Ribeiro et al. (2023) – on top of randomly sampling counterfactual treatment, we also randomly sample the ratio of modification, which could be any value such that the thickness and intensity of the counterfactual truth is in range. **The standard error of runs and violin plots of errors are reported in Appendix P.5.**

		Image MSE ↓ ($\cdot 10^{-2}$)			Thickness (th) MAE ↓			Intensity (in) MAE ↓ ($\cdot 10^{-1}$)		
	β	do(th)	do(in)	mix	do(th)	do(in)	mix	do(th)	do(in)	mix
DEAR		6.93	3.21	5.08	0.82	0.74	0.85	6.23	3.39	4.61
CHVAE	1	4.92	4.81	4.81	0.61	0.66	0.62	3.23	1.88	2.81
CHVAE	3	6.93	6.19	6.40	0.71	1.34	0.97	2.37	1.31	1.89
MED	1	2.76	0.54	1.65	0.54	0.35	0.46	1.17	0.43	0.78
MED	3	2.20	0.61	1.39	0.31	0.29	0.33	0.44	0.34	0.40
SAE (Section 2.1)		0.67	0.20	0.47	0.32	0.21	0.29	0.52	0.26	0.41
VCI (Section 2.2)		**0.42**	**0.13**	**0.36**	**0.20**	**0.14**	**0.22**	**0.42**	**0.22**	**0.33**

truth for each individual. For this reason, we specifically choose the Morpho-MNIST (Castro et al., 2019) dataset to present our main evaluation results on image generations because exact counterfactual errors can be measured even with the existence of exogenous noise, similar to the evaluations in Ribeiro et al. (2023), without having to resort to Composition, Effectiveness, and Reversibility (more details in Appendix M). Morpho-MNIST is such a dataset that, unlike other real-world datasets, the counterfactual "truth" can be computed based on the selected counterfactual treatments (modifying thickness or modifying intensity of hand-written digits). Similar to Ribeiro et al. (2023), we evaluate model constructions under single modifications as well as mix of modifications, and compare them to state-of-the-art models on high-fidelity image counterfactual generation. Contrary to Ribeiro et al. (2023), the magnitude of modification is randomly sampled, which makes the task significantly harder. The results are shown in Table 2 (standard error in Table 8) which demonstrated that ours beat state-of-the-arts by a wide margin. Note that Ribeiro et al. (2023) only evaluates mean absolute error (MAE) on thickness and intensity of counterfactual constructions, which took treatment characteristics into account but completely left out how much individuality of the original images has been preserved, whereas image MSE is a comprehensive metric that takes both factors into account and should be the primary evaluation metric when the counterfactual truth is available. To investigate the impact of counterfactual supervision and latent divergence terms in optimizations, we present an ablation study below to compare VCI to SAE and hierarchical autoencoder (HAE) with the same neural architecture.

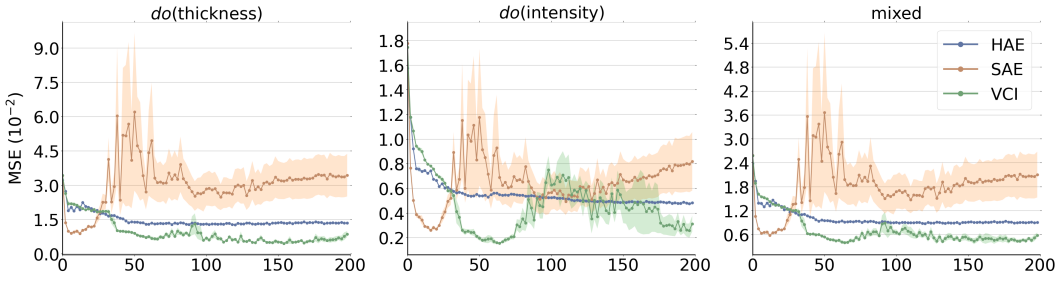

Figure 3: Ablation Study: the MSE of counterfactual construction against the truth across epochs during the training of HAE (VCI without counterfactual supervision and latent divergence), SAE (VCI without latent divergence) and VCI over five independent runs. Note that VCI with latent divergence but without counterfactual supervision does not make logical sense, but for the completeness of the ablation study, we present the results for such setting in Appendix P.2.

As can be seen in Figure 3, incorporating counterfactual supervision alone could greatly accelerate optimization in the initial epochs of training, and achieves an ideal model state in the early stage. However, although both SAE and VCI beat HAE convincingly in terms of best result, SAE is

largely unstable in the long-run without the proposed latent divergence restriction, and the full VCI optimization scheme consistently achieves better performance in terms of best result and final result. To further help the readers understand how and why the latent divergence term stabilizes the training of VCI, we include a discussion here along with some illustrations on do(intensity) in Figure 4.

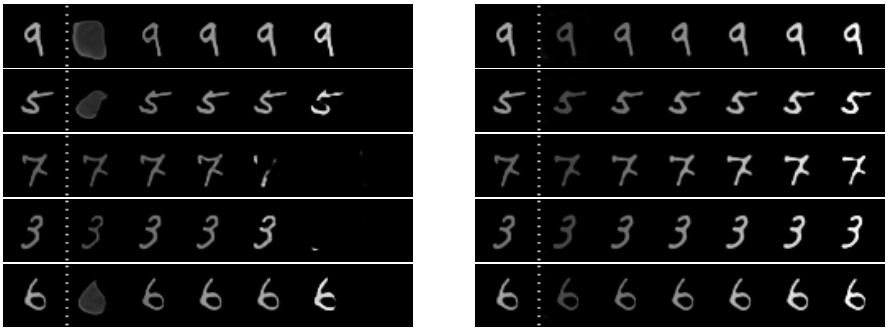

(a) SAE (b) VCI

Figure 4: Illustration of the latent divergence term's long-term impact. Samples are drawn from the last epoch of SAE and VCI on do(intensity). The left most image of each set is the original image. **More sampled results from VCI on do(thickness) and do(intensity) can be found in Figure 12.**

In a GAN training scheme, the discriminator is a neural model that could often struggle with out-of-distribution evaluations. As can be seen from the generated samples by SAE in Figure 4, when the intervention labels are close to the original label, the counterfactual generations are reasonable. For intervention labels that are significantly different from the original, the images become nonsensical. This is because the combination of an intervention label that is far from the original and an image similar to the original is highly out-of-distribution and rarely present in the observed dataset. In other words, the discriminator has never encountered an image with the same digit and style as the original having such extreme intensity variations, so whatever the generator produces, the discriminator cannot tell if it is real or fake due to the lack of reference. This results in the generator exploiting the neural discriminator in these out-of-distribution scenarios in the long run. However, the latent divergence term prevents the generator from producing these nonsensical images because, otherwise, the encoder would not be able to recover a latent distribution close to that of the original image.

3.3 CelebA-HQ

For any real-world dataset where the counterfactual truth is not available, there is not a definitive metric to evaluate how good the counterfactual constructions really are. For that reason, facial imaging datasets are prevailing benchmarks for examining counterfactual goodness because even in the lack of a quantitative metric, human can still judge the quality of counterfactuals with common sense without the need for any domain knowledge. Same as Monteiro et al. (2023), we use the CelebA-HQ (Karras et al., 2017) dataset on 64×64 resolution to evaluate the model's capability of counterfactual constructions on two factors – smiling and glasses. Some sampled results from our model are shown in Figure 5.

While MSE of the counterfactual construction cannot be measured, readers can empirically compare ours to prior work such as CHVAE (Monteiro et al., 2023) which serves as the backbone for the state-of-the-art model in high fidelity counterfactual image generation MED (Ribeiro et al., 2023). Aside from compiling counterfactual credibility across all generation tasks, ours show a strong capability of disentangling factual treatment from observed images in counterfactual construction, which can be particularly observed in the task of "removing glasses" as shown in Figure 5d. Note that contrary to prior works, we construct and supervise counterfactual outcomes during training, and the reconstruction and counterfactual construction share the same decoding mechanism. Hence, "reconstruction" is really counterfactual construction with the factual label. This can be most clearly observed in the third set of comparison in line 2 of Figure 5a, where the original image has a label of "not smiling" yet the person is really in-between smiling and not smiling. In this case, the "reconstruction" is really a counterfactual construction with treatment abiding to the original given label. Lastly, we include a discussion here regarding counterfactual fairness. Note that adding glasses

(a) Add smiling. Left: original, middle: not smiling (reconstruction), right: smiling (counterfactual).

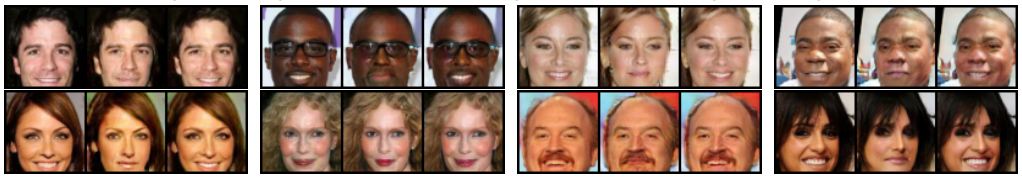

(b) Remove smiling. Left: original, middle: not smiling (counterfactual), right: smiling (reconstruction).

(c) Add glasses. Left: original, middle: no glasses (reconstruction), right: with glasses (counterfactual).

(d) Remove glasses. Left: original, middle: no glasses (counterfactual), right: with glasses (reconstruction).

Figure 5: Results on the test set of CelebA-HQ.

is a relatively easy engineering task, but relatively hard deep learning task on CelebA-HQ due to the small sample size of images with glasses. As can be seen from Figure 5c, our model not only learned to attach glasses at the right position, it also learned to attach glasses suitable to a person's style and context. However, readers may naturally start to think about the counterfactual fairness issue that might come with it, such as attaching certain type of glasses more frequently on certain race. We note that our framework can reduce spurious or unintended relations between given factors, as long as practitioners measure these factors during data collection and include them as observed labels for the composed datasets, since the learnt latent representations of our framework are encouraged to be disentangled from the observed factors. In the case of CelebA, style of glasses is unmeasured, and the model cannot reasonably tell if attaching different types of glasses on different demographics is unintended or not.

4 Conclusion

In this work, we introduced a variational Bayesian causal inference framework for estimating high-dimensional counterfactual outcomes, as well as consequent robust marginal estimators. With this framework, treatment characteristics and individuality in constructed outcomes can be explicitly balanced and optimized, and learnt latent representations are disentangled from the treatments. As for limitations, this work requires the common causal assumption that there exists no unobserved confounders, through which causal effects are identifiable. Besides, when multiple treatments are concerned, this work does not explicitly address the situation where a causal relation exists between treatments. Thus, a straightforward extension of this work could be to incorporate explicit modeling of the causal relation among treatment variables and update the descendants of given counterfactual treatment, such as Pawlowski et al. (2020), before feeding them into our counterfactual outcome construction framework.

REFERENCES

Alexander Balke and Judea Pearl. Probabilistic evaluation of counterfactual queries. In *Proceedings of the AAAI conference on artificial intelligence*, volume 12, 1994.

Yoshua Bengio, Eric Laufer, Guillaume Alain, and Jason Yosinski. Deep generative stochastic networks trainable by backprop. In *International Conference on Machine Learning*, pp. 226–234. PMLR, 2014.

Johann Brehmer, Pim De Haan, Phillip Lippe, and Taco S Cohen. Weakly supervised causal representation learning. *Advances in Neural Information Processing Systems*, 35:38319–38331, 2022.

Daniel C Castro, Jeremy Tan, Bernhard Kainz, Ender Konukoglu, and Ben Glocker. Morpho-mnist: quantitative assessment and diagnostics for representation learning. *Journal of Machine Learning Research*, 20(178):1–29, 2019.

Xi Chen, Yan Duan, Rein Houthooft, John Schulman, Ilya Sutskever, and Pieter Abbeel. Infogan: Interpretable representation learning by information maximizing generative adversarial nets. *Advances in neural information processing systems*, 29, 2016.

Rewon Child. Very deep vaes generalize autoregressive models and can outperform them on images. *arXiv preprint arXiv:2011.10650*, 2020.

Saloni Dash, Vineeth N Balasubramanian, and Amit Sharma. Evaluating and mitigating bias in image classifiers: A causal perspective using counterfactuals. In *Proceedings of the IEEE/CVF Winter Conference on Applications of Computer Vision*, pp. 915–924, 2022.

Atray Dixit, Oren Parnas, Biyu Li, Jenny Chen, Charles P Fulco, Livnat Jerby-Arnon, Nemanja D Marjanovic, Danielle Dionne, Tyler Burks, Raktima Raychowdhury, et al. Perturb-seq: dissecting molecular circuits with scalable single-cell rna profiling of pooled genetic screens. *cell*, 167(7): 1853–1866, 2016.

Ruili Feng, Jie Xiao, Kecheng Zheng, Deli Zhao, Jingren Zhou, Qibin Sun, and Zheng-Jun Zha. Principled knowledge extrapolation with gans. In *International Conference on Machine Learning*, pp. 6447–6464. PMLR, 2022.

Ian Goodfellow, Jean Pouget-Abadie, Mehdi Mirza, Bing Xu, David Warde-Farley, Sherjil Ozair, Aaron Courville, and Yoshua Bengio. Generative adversarial nets. *Advances in neural information processing systems*, 27, 2014.

Luigi Gresele, Julius Von Kügelgen, Vincent Stimper, Bernhard Schölkopf, and Michel Besserve. Independent mechanism analysis, a new concept? *Advances in neural information processing systems*, 34:28233–28248, 2021.

Hermanni Hälvä, Sylvain Le Corff, Luc Lehéricy, Jonathan So, Yongjie Zhu, Elisabeth Gassiat, and Aapo Hyvarinen. Disentangling identifiable features from noisy data with structured nonlinear ica. *Advances in Neural Information Processing Systems*, 34:1624–1633, 2021.

Jonathan Ho, Ajay Jain, and Pieter Abbeel. Denoising diffusion probabilistic models. *Advances in neural information processing systems*, 33:6840–6851, 2020.

Aapo Hyvarinen, Hiroaki Sasaki, and Richard Turner. Nonlinear ica using auxiliary variables and generalized contrastive learning. In *The 22nd International Conference on Artificial Intelligence and Statistics*, pp. 859–868. PMLR, 2019.

Tero Karras, Timo Aila, Samuli Laine, and Jaakko Lehtinen. Progressive growing of gans for improved quality, stability, and variation. *arXiv preprint arXiv:1710.10196*, 2017.

Ilyes Khemakhem, Diederik Kingma, Ricardo Monti, and Aapo Hyvarinen. Variational autoencoders and nonlinear ica: A unifying framework. In *International Conference on Artificial Intelligence and Statistics*, pp. 2207–2217. PMLR, 2020.

Hyemi Kim, Seungjae Shin, JoonHo Jang, Kyungwoo Song, Weonyoung Joo, Wanmo Kang, and Il-Chul Moon. Counterfactual fairness with disentangled causal effect variational autoencoder. In *Proceedings of the AAAI Conference on Artificial Intelligence*, volume 35, pp. 8128–8136, 2021.

Diederik P Kingma and Max Welling. Auto-encoding variational bayes. *arXiv preprint arXiv:1312.6114*, 2013.

Murat Kocaoglu, Christopher Snyder, Alexandros G Dimakis, and Sriram Vishwanath. Causalgan: Learning causal implicit generative models with adversarial training. *arXiv preprint arXiv:1709.02023*, 2017.

Aneesh Komanduri, Yongkai Wu, Feng Chen, and Xintao Wu. Learning causally disentangled representations via the principle of independent causal mechanisms. *arXiv preprint arXiv:2306.01213*, 2023.

Sébastien Lachapelle, Pau Rodriguez, Yash Sharma, Katie E Everett, Rémi Le Priol, Alexandre Lacoste, and Simon Lacoste-Julien. Disentanglement via mechanism sparsity regularization: A new principle for nonlinear ica. In *Conference on Causal Learning and Reasoning*, pp. 428–484. PMLR, 2022.

Jonathan Levy. Tutorial: Deriving the efficient influence curve for large models. *arXiv preprint arXiv:1903.01706*, 2019.

Timothy P Lillicrap, Jonathan J Hunt, Alexander Pritzel, Nicolas Heess, Tom Erez, Yuval Tassa, David Silver, and Daan Wierstra. Continuous control with deep reinforcement learning. *arXiv preprint arXiv:1509.02971*, 2015.

Francesco Locatello, Ben Poole, Gunnar Rätsch, Bernhard Schölkopf, Olivier Bachem, and Michael Tschannen. Weakly-supervised disentanglement without compromises. In *International Conference on Machine Learning*, pp. 6348–6359. PMLR, 2020.

Mohammad Lotfollahi, Anna Klimovskaia Susmelj, Carlo De Donno, Yuge Ji, Ignacio L Ibarra, F Alexander Wolf, Nafissa Yakubova, Fabian J Theis, and David Lopez-Paz. Learning interpretable cellular responses to complex perturbations in high-throughput screens. *bioRxiv*, 2021.

Christos Louizos, Uri Shalit, Joris M Mooij, David Sontag, Richard Zemel, and Max Welling. Causal effect inference with deep latent-variable models. *Advances in neural information processing systems*, 30, 2017.

Miguel Monteiro, Fabio De Sousa Ribeiro, Nick Pawlowski, Daniel C Castro, and Ben Glocker. Measuring axiomatic soundness of counterfactual image models. *arXiv preprint arXiv:2303.01274*, 2023.

Thomas M Norman, Max A Horlbeck, Joseph M Replogle, Alex Y Ge, Albert Xu, Marco Jost, Luke A Gilbert, and Jonathan S Weissman. Exploring genetic interaction manifolds constructed from rich single-cell phenotypes. *Science*, 365(6455):786–793, 2019.

Nick Pawlowski, Daniel Coelho de Castro, and Ben Glocker. Deep structural causal models for tractable counterfactual inference. *Advances in Neural Information Processing Systems*, 33: 857–869, 2020.

Judea Pearl. *Probabilistic reasoning in intelligent systems: networks of plausible inference*. Morgan kaufmann, 1988.

Judea Pearl. Causal diagrams for empirical research. *Biometrika*, 82(4):669–688, 1995.

Judea Pearl. *Causality*. Cambridge university press, 2009.

Fabio De Sousa Ribeiro, Tian Xia, Miguel Monteiro, Nick Pawlowski, and Ben Glocker. High fidelity image counterfactuals with probabilistic causal models. *arXiv preprint arXiv:2306.15764*, 2023.

James Robins. A new approach to causal inference in mortality studies with a sustained exposure period—application to control of the healthy worker survivor effect. *Mathematical modelling*, 7 (9-12):1393–1512, 1986.

Paul R Rosenbaum and Donald B Rubin. The central role of the propensity score in observational studies for causal effects. *Biometrika*, 70(1):41–55, 1983.

Pedro Sanchez and Sotirios A Tsaftaris. Diffusion causal models for counterfactual estimation. *arXiv preprint arXiv:2202.10166*, 2022.

Axel Sauer and Andreas Geiger. Counterfactual generative networks. *arXiv preprint arXiv:2101.06046*, 2021.

Ralf Schmidt, Zachary Steinhart, Madeline Layeghi, Jacob W Freimer, Raymund Bueno, Vinh Q Nguyen, Franziska Blaeschke, Chun Jimmie Ye, and Alexander Marson. Crispr activation and interference screens decode stimulation responses in primary human t cells. *Science*, 375(6580): eabj4008, 2022.

John Schulman, Filip Wolski, Prafulla Dhariwal, Alec Radford, and Oleg Klimov. Proximal policy optimization algorithms. *arXiv preprint arXiv:1707.06347*, 2017.

Xinwei Shen, Furui Liu, Hanze Dong, Qing Lian, Zhitang Chen, and Tong Zhang. Weakly supervised disentangled generative causal representation learning. *The Journal of Machine Learning Research*, 23(1):10994–11048, 2022.

Rui Shu, Yining Chen, Abhishek Kumar, Stefano Ermon, and Ben Poole. Weakly supervised disentanglement with guarantees. *arXiv preprint arXiv:1910.09772*, 2019.

Kihyuk Sohn, Honglak Lee, and Xinchen Yan. Learning structured output representation using deep conditional generative models. *Advances in neural information processing systems*, 28, 2015.

Peter Spirtes, Clark N Glymour, and Richard Scheines. *Causation, prediction, and search*. MIT press, 2000.

Sanjay R Srivatsan, José L McFaline-Figueroa, Vijay Ramani, Lauren Saunders, Junyue Cao, Jonathan Packer, Hannah A Pliner, Dana L Jackson, Riza M Daza, Lena Christiansen, et al. Massively multiplex chemical transcriptomics at single-cell resolution. *Science*, 367(6473):45–51, 2020.

Cathie Sudlow, John Gallacher, Naomi Allen, Valerie Beral, Paul Burton, John Danesh, Paul Downey, Paul Elliott, Jane Green, Martin Landray, et al. Uk biobank: an open access resource for identifying the causes of a wide range of complex diseases of middle and old age. *PLoS medicine*, 12(3): e1001779, 2015.

Arash Vahdat and Jan Kautz. Nvae: A deep hierarchical variational autoencoder. *Advances in neural information processing systems*, 33:19667–19679, 2020.

Mark J Van Der Laan and Daniel Rubin. Targeted maximum likelihood learning. *The international journal of biostatistics*, 2(1), 2006.

Aad W Van der Vaart. *Asymptotic statistics*, volume 3. Cambridge university press, 2000.

Hado Van Hasselt, Arthur Guez, and David Silver. Deep reinforcement learning with double q-learning. In *Proceedings of the AAAI conference on artificial intelligence*, volume 30, 2016.

Pascal Vincent, Hugo Larochelle, Yoshua Bengio, and Pierre-Antoine Manzagol. Extracting and composing robust features with denoising autoencoders. In *Proceedings of the 25th international conference on Machine learning*, pp. 1096–1103, 2008.

Athanasios Vlontzos, Bernhard Kainz, and Ciarán M Gilligan-Lee. Estimating categorical counterfactuals via deep twin networks. *Nature Machine Intelligence*, 5(2):159–168, 2023.

Julius von Kügelgen, Michel Besserve, Wendong Liang, Luigi Gresele, Armin Kekić, Elias Bareinboim, David M Blei, and Bernhard Schölkopf. Nonparametric identifiability of causal representations from unknown interventions. *arXiv preprint arXiv:2306.00542*, 2023.

Yulun Wu, Layne C Price, Zichen Wang, Vassilis N Ioannidis, Robert A Barton, and George Karypis. Variational causal inference. *arXiv preprint arXiv:2209.05935*, 2022.

Mengyue Yang, Furui Liu, Zhitang Chen, Xinwei Shen, Jianye Hao, and Jun Wang. Causalvae: Disentangled representation learning via neural structural causal models. In *Proceedings of the IEEE/CVF conference on computer vision and pattern recognition*, pp. 9593–9602, 2021.

Jinsung Yoon, James Jordon, and Mihaela Van Der Schaar. Ganite: Estimation of individualized treatment effects using generative adversarial nets. In *International Conference on Learning Representations*, 2018.

Jiageng Zhu, Hanchen Xie, Jianhua Wu, Jiazhi Li, Mahyar Khayatkhoei, Mohamed E Hussein, and Wael AbdAlmageed. Shadow datasets, new challenging datasets for causal representation learning. *arXiv preprint arXiv:2308.05707*, 2023.

A Introduction on Latent Disentanglement

The study of latent disentanglement in deep causal modeling has mainly focused on two areas. Most prior works lie in the first area that is causal representation learning, in which researchers seek to learn latent variables corresponding to true causal factors and identify the structure of their causal relations (Yang et al., 2021; Hälvä et al., 2021; Gresele et al., 2021; Lachapelle et al., 2022; Komanduri et al., 2023), predominantly leveraging recent advances in non-linear independent component analysis (ICA) (Hyvarinen et al., 2019; Khemakhem et al., 2020) and identify causal structure up to Markov equivalence (Spirtes et al., 2000) or graph isomorphism under rather heavy assumptions. The second area and the area this work is concerned of is counterfactual generative modeling, in which the focus is to conduct disentangled exogenous noise abduction that aids counterfactual outcome generation (Lotfollahi et al., 2021; Shen et al., 2022). In this context, the goal is to acquire latent representations disentangled from the observed treatment to aid the correct identification of the causal effect of counterfactual treatments.

B Comparison of Conditional VAE and VCI

For readers that are more familiar with deep generative modeling than causal inference, we provide a straightforward comparison between conditional VAE and VCI (fundamentally a comparison between conditional generative modeling and counterfactual generative modeling) in this section using VAE's notations. For data x and condition c, the differences in formulations and objectives are shown in Figure 6 and Table 3. In causal inference, counterfactual outcome is an individual-level concept – for a given individual that we observed outcome/data x under treatment/condition c, what would their outcome have been if they had received treatment/condition c' instead? This is a "would have" question, meaning that we seek to find out what the alternative outcome x' would be in a parallel world where everything in the state of the universe remained the same, except that the treatment c' (and its impact) was different. With this in mind, it is not hard to see why the conditional generative modeling formulation is unorthodox for counterfactual generative modeling – the ELBO serves to optimize the marginal-level (interventional) likelihood $p(x|c)$ and the learnt model generates samples towards the marginal-level (interventional) distribution $p(x|c)$ during inference time, and the question being asked here is "what will an outcome x be under condition c?". This is a "will" question – it is generating *any* outcome under condition c, not given a specific individual, not given a specific state of the universe. Therefore, contrary to prior works in HVAEs and diffusion models (Sanchez & Tsaftaris, 2022; Monteiro et al., 2023; Ribeiro et al., 2023) which focus on model design adaptations to make the conditional VAE formulation work in counterfactual generative modeling, we first derive the orthodox formulation and objective for counterfactual generative modeling, then make the necessary model designs afterwards according to the newly derived ELBO.

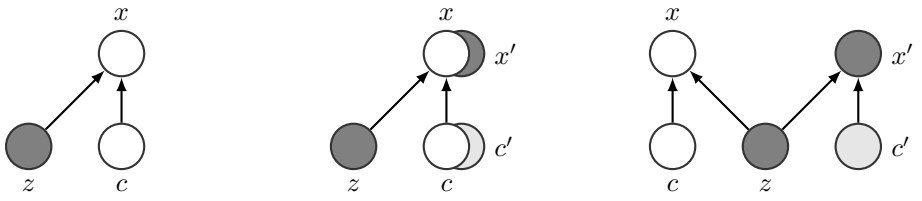

(a) VAE (b) VCI (c) VCI (unfolded)

Figure 6: The data generating formulation of conditional generative modeling under VAE formulation and counterfactual generative modeling under VCI formulation using standard VAE notations. $p(x|z,c) = p(x'|z,c')$ for $c = c'$. White nodes are observed, light grey nodes are assigned during training and inference, dark grey nodes are unobserved.

As can be seen in Table 3, the difference in motivations between the two objectives manifest themselves in the derived ELBO in some intuitive ways: VAE does not have the motivation to maximize counterfactual outcome likelihood, hence no such term $\log[\hat{p}(x'_{\theta,\phi}|c')]$ to perform counterfactual supervision; VCI does not have the motivation to denoise or to generate samples from pure noise duing inference time, hence no such term $D_{\mathrm{KL}}[q_\phi(z|x,c) \parallel p_\theta(z|c)]$ to bound latent distribution on some marginal prior.

Table 3: The objective and ELBO for conditional generative modeling under VAE formulation and counterfactual generative modeling under VCI formulation using standard VAE notations. As illustrated in Section 2.2, the latent divergence term in VCI is directly derived from the causal objective and serves a causal purpose that is entirely different from the prior latent bounding purpose of VAE.

	VAE	VCI
Objective	$p(x\|c)$	$p(x'\|x,c,c')$
ELBO	$J^{\text{VAE}}_{\theta,\phi}(x,c) = \mathbb{E}_{q_\phi(z\|x,c)} \log [p_\theta(x\|z,c)] - D_{\text{KL}} \left[q_\phi(z\|x,c) \parallel p_\theta(z\|c) \right]$	$J^{\text{VCI}}_{\theta,\phi}(x,c,c') = \mathbb{E}_{q_\phi(z\|x,c)} \log [p_\theta(x\|z,c)] + \log \left[\hat{p}(x'_{\theta,\phi}\|c') \right] - D_{\text{KL}} \left[q_\phi(z\|x,c) \parallel q_\phi(z\|x'_{\theta,\phi},c') \right]$

B.1 Diffusion Models

Due to the popularity of the diffusion models (Ho et al., 2020), we feel the necessity to include a discussion here specifically about its compatibility with counterfactual generative modeling. It is very important to note that, although diffusion model is the state-of-the-art in generative and conditional generative modeling, it has not been shown that it has better capability in counterfactual generative modeling than ordinary HVAEs with learnable encoder (Monteiro et al., 2023; Ribeiro et al., 2023), and the reason is straightforward once the readers truly understand the fundamental incompatibility between the goal of counterfactual generative modeling and the diffusion mechanism. As discussed above, the heart and soul of counterfactual generative modeling, in contrast to conditional generative modeling, is the abduction of exogenous noise. The diffusion mechanism, on the other hand, inherently contradicts exogenous noise abduction: not only does it work towards the wrong interventional objective as a model under the VAE formulation, the individuality contained in the factual outcome is also guaranteed to be discarded under the unlearable diffusing encoder. Prior works that attempted at utilizing diffusion models in counterfactual generative modeling (Dash et al., 2022; Sanchez & Tsaftaris, 2022) clearly exhibited this flaw: as can be seen from the CelebA results in Dash et al. (2022), exogenous noise/individuality has been largely discarded in counterfactual generation – because the diffusion model is doing what it is intended to do: diffusing exogenous and generating samples that fit seeminglessly into the conditional/marginal likelihood $p(x|c)$; Sanchez & Tsaftaris (2022) on the other hand, hardly showed any evidence that the model is capable of preserving exogenous noise/individuality – MNIST was the only benchmark in their experiments and only intervening digit was performed, which does not have measurable counterfactual truth as intervening thickness and intensity in Morpho-MNIST (in general, the interventions performed in Sanchez & Tsaftaris (2022) all drastically changed the objects in the original images, which makes it quite impossible to tell whether exogenous noise are preserved either quantitatively or qualitatively). We want to clarify that we think Dash et al. (2022) and Sanchez & Tsaftaris (2022) are meaningful and well-written works that conducted the important advancement of experimenting diffusion models in counterfactual generative modeling, however, diffusion models have not shown the capability of exogenous noise abduction on the level of state-of-the-art HVAEs (Monteiro et al., 2023; Ribeiro et al., 2023) as it stands.

C Related Work

Key prior works in deep causal generative modeling fall primarily into three categories: variational-based methods **CEVAE** (Louizos et al., 2017), **DeepSCM** (Pawlowski et al., 2020), **DiffSCM** (Sanchez & Tsaftaris, 2022), **CHVAE** (Monteiro et al., 2023), **MED** (Ribeiro et al., 2023); adversarial-based methods **CausalGAN** (Kocaoglu et al., 2017), **GANITE** (Yoon et al., 2018); hybrid method **DEAR** (Shen et al., 2022) as well as our framework **VCI**. A comparative analysis of ours against these related works can be found in Table 4.

CEVAE uses variational autoencoders (VAEs) to infer latent confounders and estimate individual treatment effects (ITE). **DeepSCM** integrates deep learning into SCMs using normalizing flows and variational inference for counterfactual inference. **DiffSCM** leverages generative diffusion models, using forward and reverse diffusion processes guided by anti-causal predictors to generate counterfactuals. **CHVAE** extends VDVAE to a conditional model, performing abduction by encoding

images and parent attributes, and includes a penalty for counterfactual conditioning. **MED** uses hierarchical VAEs with deep causal mechanisms, inferring exogenous noise by conditioning on observed data and parent variables. **GANITE** uses a counterfactual generator to create proxies for unobserved outcomes and an ITE generator to estimate potential outcomes. **DEAR** combines a VAE-like generative loss with a supervised loss in a bidirectional generative model, trained with a GAN algorithm requiring knowledge of the causal graph structure and extra labels for latent factors.

As illustrated in Section 2 and Appendix B, the primary contribution of our framework **VCI** is the revolution of VAE formulation which leads to a brand new stochastic optimization scheme that optimizes the ELBO of an actual counterfactual objective. This brings about end-to-end counterfactual supervision and exogenous noise disentanglement as presented in Table 4.

Table 4: A comparative analysis of related work. "Variational Objective Distribution" describes the objective that the ELBOs are derived for in a variational-based method: "Joint" indicates joint distributions such as $p(y, x, t)$ or $p(y, z)$ (note that different works could have different notations, here we use y, x, t, z to represent outcome, covariates, treatment, latent respectively), and "Interventional" indicates conditional outcome distribution $p(y|x, t)$ or $p(y|t)$. "Marginal Distribution Alignment" describes whether the stochastic optimization objective involves mechanisms that match the distribution of outcome constructions with some learnt marginal outcome distribution.

	Type	Variational Objective Distribution	Hierarchical Model Structure	Marginal Distribution Alignment	Causal Discovery	End-to-End Counterfactual Supervision	Latent Disentanglement
CEVAE	Variational	Joint	✗	✗	✓	✗	✗
CausalGAN	Adversarial	–	✗	✓	✗	✗	✗
GANITE	Adversarial	–	✗	✓	✗	✗	✗
DEAR	Variational + Adversarial	Joint	✗	✗	✓	✗	*
DeepSCM	Variational	Interventional	✗	✗	✗	✗	✗
DiffSCM	Variational	Interventional	✓	✗	✗	✗	✗
CHVAE	Variational	Interventional	✓	✗	✗	✗	✗
MED	Variational	Interventional	✓	✓	✗	✗	✗
VCI	Variational + Adversarial	Counterfactual	✓	✓	✗	✓	✓

*DEAR learns restrictive representation for latent z (z is disentangled from treatment t when encoding t) but does not learn consistent representation for z (t is not disentangled from z when encoding z).

D Comparison of traditional causal formulation and VCI formulation

We note that we formulate counterfactuals Y' and T' as separate variables for the cleanliness of graphical model and notation simplicity in variational inference, with the goal to bridge readers with variational inference background and causal inference background. In essence, it is no different from the traditional causal formulation where the $\mathrm{do}()$ operation is directly imposed on factual variable T, as T' is just a dummy variable with no observations. Denote $Y_{\mathrm{do}(T=t')}$ as $Y_{t'}$, see Figure 7 for a demonstration of our formulation in traditional notations.

Then under the ignorability assumption (Assumption 1, note that there is no ϵ_Y and ϵ'_Y in the traditional SCM formulation as there is only one copy of exogenous noise U_Y injected to factual and counterfactual outcome, but in general if there exists ϵ_Y and ϵ'_Y independent of U_Y, the following result holds as long as $\epsilon_Y, \epsilon'_Y \perp\!\!\!\perp U_T$), we have the following version of Theorem 1:

Corollary 2. *Suppose a collection of random variables follows a causal structure defined by the Bayesian network in Figure 7b. Then* $\log[p(Y_{t'}|Y, X, T, t')]$ *has the following variational lower bound:*

$$\log\left[p(Y_{t'}|Y, X, T, t')\right] \geq \mathbb{E}_{p(Z|Y,T,X)} \log\left[p(Y|Z, T)\right] - D\left[p(Y|X, T) \parallel p(Y_{t'}|X, t')\right] - D_{\mathrm{KL}}\left[p(Z|Y, T, X) \parallel p(Z|Y_{t'}, t', X)\right] \tag{10}$$

where $D[p \parallel q] = \log p - \log q$.

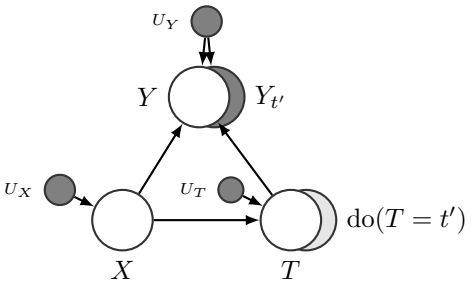

(a) SCM, traditional

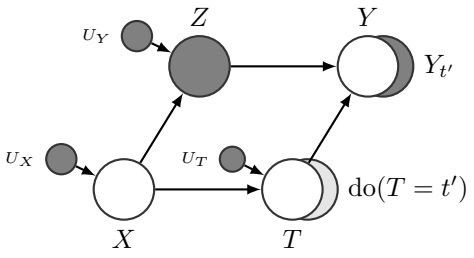

(b) SCM, with $f_Y(X, T, U_Y) = \tilde{f}_Y(f_Z(X, U_Y), T)$

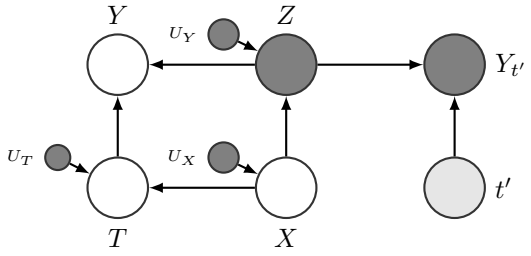

(c) SCM, with $f_Y(X, T, U_Y) = \tilde{f}_Y(f_Z(X, U_Y), T)$, unfolded

Figure 7: The evolution of our formulation from traditional SCM with observed triplets (X, T, Y). Figure 7b is simply extending the production function towards Y with an intermediate variable Z representing two of its inputs (when $f_Z(X, U_Y) = (X, U_Y)$, $\tilde{f}_Y$ is just f_Y). Then, Figure 7c is just the unfolded graphical model of Figure 7b, as the $\mathrm{do}()$ operation replaces T in the production function of Y with t', i.e. $Y_{t'} = f_Y(X, t', U_Y)$.

Now we define dummy variables $T' = f_T(X, U'_T)$, with U'_T satisfying the ignorability assumption (Remark 1), and $Y' = f_Y(X, T', U_Y) = \tilde{f}_Y(f_Z(X, U_Y), T')$. Then, $Y'_{\mathrm{do(T'=t')}} = f_Y(X, t', U_Y) = Y_{t'}$. Hence, we have $p(Y_{t'}|Y, X, T, t') = p(Y'|Y, X, T, do(T' = t')) = p(Y'|Y, X, T, T' = t')$ for any t'. Therefore, Figure 1a and Theorem 1 is in essence just Figure 7c and Corollary 2 with different notations and variable definitions.

E Implicit Counterfactual Supervision

We demonstrated in the previous section that the marginal-level observed likelihood is unorthodox for counterfactual generative modeling and the individual-level likelihood $\log[p(Y'|Y, X, T, T')]$ is better motivated for this task. However, for researchers that insist to work towards the traditional likelihood objective $\log[p(Y|X, T)]$ composed only of observed variables, there is an approach to conduct counterfactual supervision implicitly – to view Y' as a latent variable restricted on the prior $p(Y'|X, T')$ and view counterfactual construction task as a latent recognition task:

Proposition 3. *$J(O) = \log[p(Y|X, T)]$ has the following variational lower bound:*

$$\begin{aligned} J(O) \geq\ & \mathbb{E}_{p(Z|Y,T,X)} \log\left[p(Y|Z, T)\right] - \mathbb{E}_{p(Z|Y,T,X)} D_{\mathrm{KL}}\left[p(Y'|Z, T') \parallel p(Y'|X, T')\right] \\ & - D_{\mathrm{KL}}\left[p(Z|Y, T, X)p(Y'|Z, T') \parallel p(Z|Y', T', X)p(Y'|Z, T')\right]. \end{aligned} \tag{11}$$

which induces the following ELBO in stochastic optimization:

$$\begin{aligned} J_{\theta,\phi}(o) =\ & \mathbb{E}_{q_\phi(z|y,t,x)} \log\left[p_\theta(y|z, t)\right] - \mathbb{E}_{q_\phi(z|y,t,x)} D_{\mathrm{KL}}\left[p_\theta(Y'|z, t') \parallel \hat{p}(Y'|x, t')\right] \\ & - D_{\mathrm{KL}}\left[q_\phi(Z|y, t, x)p_\theta(Y'|Z, t') \parallel q_\phi(Z|Y', t', x)p_\theta(Y'|Z, t')\right]. \end{aligned} \tag{12}$$

Equation 12 avoids estimating Y' with a single sample as in the objective (Equation 3) derived from the explicit ELBO (Equation 2). However, it could be a lot more sampling inefficient as the divergence term requires Monte-Carlo samples from both Z and Y' to be estimated.

F Definition of Consistence, Restrictiveness, and Disentanglement

Let $\mathcal{H} = \{(\tilde{p}, \tilde{q}) \mid \tilde{p} : \mathcal{S} \to [0,1]^{\Sigma_\mathcal{V}},\ \tilde{q} : \mathcal{V} \times \mathcal{X} \to [0,1]^{\Sigma_\mathcal{S}}\}$ be a hypothesis class of stochastic models $(\tilde{p}, \tilde{q})$. The input space of $\tilde{p}$ is a measurable space $\mathcal{S}$ where a feature vector $s \in \mathcal{S}$ is drawn; the input space of $\tilde{q}$ is the product space of $\mathcal{V}$ and $\mathcal{X}$ where a vector of interest $v \in \mathcal{V}$ and some auxiliary attributes $x \in \mathcal{X}$ are drawn. The outputs of $\tilde{p}$ and $\tilde{q}$ are probability measures on $\mathcal{V}$ and $\mathcal{S}$ respectively. Let the true model (p^*, q^*) be the true conditional distributions $(p_0(V|s), p_0(S|v,x))$ of random variables V and S. The following definitions provide criteria under which two parts S_I and $S_{\setminus I}$ of feature variable S separated by a index set I are disentangled by a model.

Definition 1 (Consistence). *Consider $s = (s_I, s_{\setminus I})$ and $s' = (s_I, s'_{\setminus I})$ where*

$$x \sim p(X) \tag{13}$$

$$s_I \sim p(S_I|x) \tag{14}$$

$$s_{\setminus I}, s'_{\setminus I} \overset{\text{iid}}{\sim} p(S_{\setminus I}|s_I, x) \tag{15}$$

We say that $\tilde{q}$ is consistent with S_I if p is the true distribution p_0 and

$$\mathbb{E}_{p_0,p^*} \|\tilde{q}_I \circ p^*(s;x) - \tilde{q}_I \circ p^*(s';x)\| = 0. \tag{16}$$

More generally, we say that $(\tilde{p}, \tilde{q})$ is consistent with S_I under p if

$$\mathbb{E}_{p,\tilde{p}} \|\tilde{q}_I \circ \tilde{p}(s;x) - \tilde{q}_I \circ \tilde{p}(s';x)\| = 0. \tag{17}$$

As discussed in Shu et al. (2019), consistence states that for any fixed choice of S_I, resampling $S_{\setminus I}$ should not affect the oracle's measurement of S_I (note that we call consistency in Shu et al. (2019) as consistence in this work to not be confused with the notion of consistency in causal inference). A more general notion of consistence is defined in addition, as it is valuable in real-world optimization to evaluate the estimating model's consistence under its own oracle $\tilde{q} \circ \tilde{p}$.

In contrast, restrictiveness states that for any fixed choice of $S_{\setminus I}$, resampling S_I should not affect the oracle's measurement of $S_{\setminus I}$:

Definition 2 (Restrictiveness). *Consider $s = (s_I, s_{\setminus I})$ and $s' = (s'_I, s_{\setminus I})$ where*

$$x \sim p(X) \tag{18}$$

$$s_{\setminus I} \sim p(S_{\setminus I}|x) \tag{19}$$

$$s_I, s'_I \overset{\text{iid}}{\sim} p(S_I|s_{\setminus I}, x) \tag{20}$$

We say that $\tilde{q}$ is restricted to S_I if p is the true distribution p_0 and

$$\mathbb{E}_{p_0,p^*} \|\tilde{q}_{\setminus I} \circ p^*(s;x) - \tilde{q}_{\setminus I} \circ p^*(s';x)\| = 0. \tag{21}$$

More generally, we say that $(\tilde{p}, \tilde{q})$ is restricted to S_I under p if

$$\mathbb{E}_{p,\tilde{p}} \|\tilde{q}_{\setminus I} \circ \tilde{p}(s;x) - \tilde{q}_{\setminus I} \circ \tilde{p}(s';x)\| = 0. \tag{22}$$

Notice that the consistence and restrictiveness of S_I is equivalent to the restrictiveness and consistence of $S_{\setminus I}$, we have the following definition of disentanglement:

Definition 3 (Disentanglement). *We say that $\tilde{q}$ disentangles S_I and $S_{\setminus I}$ if $\tilde{q}$ is consistent with and restricted to S_I. More generally, we say that $(\tilde{p}, \tilde{q})$ disentangles S_I and $S_{\setminus I}$ under p if $(\tilde{p}, \tilde{q})$ is consistent with and restricted to S_I under p.*

G Robust Marginal Effect Estimation

By Van der Vaart (2000), a sequence of estimators $\hat{\Psi}_n$ is asymptotically efficient if $\sqrt{n}(\hat{\Psi}_n - \Psi(p)) = 1/\sqrt{n}\sum_{k=1}^{n} \tilde{\psi}_p(W_k) + o_p(1)$ where $\tilde{\psi}_p$ is the efficient influence function of $\Psi(p)$ and $W_k \sim p(W)$. The theorem below gives this efficient influence function for the average treatment effect of the treated (ATT) $\Psi(p) = \mathbb{E}_p[Y'_{\text{do}(T'=\alpha)}]$ and thus provides a construction of an asymptotically efficient regular estimator for Ψ:

Theorem 2. *Suppose $W : \Omega \to \mathcal{R}_W$ follows a causal structure defined by the Bayesian network in Figure 1, where the counterfactual conditional distribution $p(Y', T'|Z, X)$ is identical to that of its factual counterpart $p(Y, T|Z, X)$. Then $\Psi(p)$ has the following efficient influence function:*

$$\tilde{\psi}_p(W) = \frac{I(T = \alpha)}{p(T|X)}(Y - \mathbb{E}_p[Y|Z, T]) + \mathbb{E}_p[Y'|Z, T' = \alpha] - \Psi. \tag{23}$$

This leads to the construction of $\hat{\Psi}_n(o)$ in Equation 4 which is asymptotically efficient under some regularity conditions (Van Der Laan & Rubin, 2006), with the asymptotic distribution given by

$$\sqrt{n}(\hat{\Psi}_n - \Psi(p)) \xrightarrow{d} \mathcal{N}(0, E_p\left[\tilde{\psi}_p(W)\tilde{\psi}_p(W)^T\right]) \tag{24}$$

where the variance can be estimated empirically in practice and confidence bounds can be constructed accordingly. The robust estimator within the VCI framework can also be extended to estimating covariate-specific marginal treatment effect $\Xi(p) = \mathbb{E}_p[Y'_{\text{do}(X=c,T'=\alpha)}]$ for a given covariate c of interest:

Corollary 3. *Under the same settings as Theorem 3, $\Xi(p)$ has the following efficient influence function:*

$$\tilde{\xi}_p(W) = \frac{I(X = c)}{p(X)}\tilde{\psi}_p(W). \tag{25}$$

Note that when $p(X)$ is estimated empirically, the asymptotically efficient estimator for $\Xi(p)$:

$$\hat{\Xi}_n(o) = \frac{1}{n}\sum_{i=1}^{n}\frac{I(x_k = c)}{\hat{p}(x_k)}\left\{\frac{I(t_k = \alpha)}{\hat{e}(t_k|x_k)} \cdot y_k + \left(1 - \frac{I(t_k = \alpha)}{\hat{e}(t_k|x_k)}\right) \cdot \mathbb{E}_{p_\theta}[Y'|z_{k,\phi}, T' = \alpha]\right\} \tag{26}$$

$$= \frac{1}{n_c}\sum_{i=1}^{n_c}\left\{\frac{I(t_{k_i} = \alpha)}{\hat{e}(t_{k_i}|x_{k_i})} \cdot y_{k_i} + \left(1 - \frac{I(t_{k_i} = \alpha)}{\hat{e}(t_{k_i}|x_{k_i})}\right) \cdot \mathbb{E}_{p_\theta}[Y'|z_{k_i,\phi}, T' = \alpha]\right\} \tag{27}$$

is simply an application of Equation 4 on the set of observations with covariates c, where $\{k_1, k_2, \ldots, k_{n_c}\}$ are indices such that $x_{k_i} = c$.

H Formal Definition of Common Causal Assumptions under the VCI Formulation

Assumption 1 (Ignorability)**.** *There is no unobserved confounders, i.e. $\tilde{U}_Y \perp\!\!\!\perp U_T$, where $\tilde{U}_Y = (U_Y, \epsilon_Y, \epsilon'_Y)$.*

Note that this assumption can be extended to the counterfactual treatment variable T' w.o.l.g.:

Remark 1 (Ignorability)**.** *Note that T' in our formulation is a dummy variable with no observations, and we only care about the outcome distribution of Y' under assignment $do(T' = t')$ for any given t'. Hence, the ignorability $\tilde{U}_Y \perp\!\!\!\perp U'_T$, and in addition, $U_X \perp\!\!\!\perp U'_T$, can be assumed w.o.l.g. just so that the outcome distributions under $do(T' = t')$ reduces to that under $T' = t'$ conditioned on X or Z for notation simplicity, without violating any actual mechanism on the observed data.*

The ignorability assumption is universally assumed and entailed in our formulation in Figure 1.

Assumption 2 (Consistency)**.** *An individual's observed outcome under a treatment is the same as its potential outcome under that treatment, i.e. $Y = Y'_{\text{do}(T'=T)}$, where $Y'_{\text{do}(T'=T)} = f_Y(Z, T, \epsilon'_Y)$ is yielded by replacing the production equation for T' with $T' = T$.*

The consistency assumption, commonly stated in causal inference literature, is indeed an assumption and not just a direct consequence of the SCM under our formulation, since ϵ_Y and ϵ'_Y are two copies of independent variables. In essence, it states that $\epsilon_Y = 0$ and there is only one copy of exogenous noise U_Y injected to Y and Y':

Remark 2 (Consistency)**.** *Under the consistency assumption, $f_Y(z, t, \epsilon_Y)$ must be deterministic for any z and t, otherwise we would have $Y \neq Y'_{\text{do}(T'=T)}$ since $f_Y(z, t, \epsilon_Y)$ and $f_Y(z, t, \epsilon'_Y)$ are independent for any z and t. Hence there exists deterministic function $\tilde{f}_Y$ such that $\tilde{f}_Y(Z, T, 0) = f_Y(Z, T, \epsilon_Y)$. So w.o.l.g., we let $\epsilon_Y = 0$ under the consistency assumption.*

Note that this assumption does not result in a collapse of counterfactual inference to interventional inference in the traditional sense, as latent Z is unobserved and entails further uncertainty U_Y beyond the observed covariates X.

I Proof of Theoretical Results

I.1 Evidence Lower Bound

I.1.1 Proof of Theorem 1

Proof. By the d-separation (Pearl, 1988) of paths on the causal graph defined in Figure 1a, we have

$$\log\left[p(Y'|Y,X,T,T')\right] = \log \mathbb{E}_{p(Z|Y,T,X)}\left[p(Y'|Z,Y,X,T,T')\right] \tag{28}$$

$$\geq \mathbb{E}_{p(Z|Y,T,X)} \log\left[p(Y'|Z,Y,X,T,T')\right] \quad \text{(Jensen's inequality)} \tag{29}$$

$$= \mathbb{E}_{p(Z|Y,T,X)} \log \frac{p(Y',Z|Y,X,T,T')}{p(Z|Y,T,X)} \tag{30}$$

$$= \mathbb{E}_{p(Z|Y,T,X)} \log \frac{p(Y',Z,Y|X,T,T')}{p(Z|Y,T,X)p(Y|X,T)} \tag{31}$$

$$= \mathbb{E}_{p(Z|Y,T,X)} \log \frac{p(Y|Z,T)p(Z|Y',T',X)p(Y'|X,T')}{p(Z|Y,T,X)p(Y|X,T)} \tag{32}$$

$$\begin{aligned} &= \mathbb{E}_{p(Z|Y,T,X)} \log\left[p(Y|Z,T)\right] - D_{\mathrm{KL}}\left[p(Z|Y,T,X) \parallel p(Z|Y',T',X)\right] \\ &\quad - D\left[p(Y|X,T) \parallel p(Y'|X,T')\right]. \end{aligned} \tag{33}$$

Note that the above steps still hold with an additional edge from Z or T to X (but not both) if U_Y or U_T is dependent of U_X. □

I.1.2 Proof of Proposition 3

Proof. By the d-separation (Pearl, 1988) of paths on the causal graph defined in Figure 1a, we have

$$\log\left[p(Y|X,T)\right] = \log\left[p(Y|X,T,T')\right] = \log \mathbb{E}_{p(Z,Y'|Y,X,T,T')} \frac{p(Y,Z,Y'|X,T,T')}{p(Z,Y'|Y,X,T,T')} \tag{34}$$

$$\geq \mathbb{E}_{p(Z,Y'|Y,X,T,T')} \log \frac{p(Y,Z,Y'|X,T,T')}{p(Z,Y'|Y,X,T,T')} \quad \text{(Jensen's inequality)} \tag{35}$$

$$= \mathbb{E}_{p(Z,Y'|Y,X,T,T')} \log \frac{p(Y'|X,T')p(Y,Z|Y',X,T,T')}{p(Z,Y'|Y,X,T,T')} \tag{36}$$

$$= \mathbb{E}_{p(Z,Y'|Y,X,T,T')} \log \frac{p(Y'|X,T')p(Z|Y',T',X)p(Y|Z,T)}{p(Z|Y,T,X)p(Y'|Z,T')} \tag{37}$$

$$= \mathbb{E}_{p(Z,Y'|Y,X,T,T')} \log \frac{p(Y'|X,T')p(Z|Y',T',X)p(Y'|Z,T')p(Y|Z,T)}{p(Y'|Z,T')p(Z|Y,T,X)p(Y'|Z,T')} \tag{38}$$

$$\begin{aligned} &= -\mathbb{E}_{p(Z|Y,T,X)} D_{\mathrm{KL}}\left[p(Y'|Z,T') \parallel p(Y'|X,T')\right] \\ &\quad - D_{\mathrm{KL}}\left[p(Z|Y,T,X)p(Y'|Z,T') \parallel p(Z|Y',T',X)p(Y'|Z,T')\right] \\ &\quad + \mathbb{E}_{p(Z|Y,T,X)} \log\left[p(Y|Z,T)\right]. \end{aligned} \tag{39}$$

Note that the above steps still hold with an additional edge from Z or T to X (but not both) if U_Y or U_T is dependent of U_X. □

I.1.3 Proof of Corollary 2

Proof. Note that Theorem 1 only relies on the conditional dependency structure in Figure 1, and the only difference between the dependency structure of (X,Z,T,T',Y,Y') in Figure 1 and that of $(X,Z,T,t',Y,Y_{t'})$ in Figure 7 is the dependency between (X,T') and (X,t'). However, such difference does not change the conditional independence of latent posterior: $p(Z|Y,T,X,t') =$

$p(Z|Y,T,X)$ and $p(Z|Y_{t'},t',X,T) = p(Z|Y_{t'},t',X)$, the conditional independence of outcome distribution $p(Y|Z,T,t') = p(Y|Z,T)$ and $p(Y_{t'}|Z,t',T) = p(Y_{t'}|Z,t')$, and the conditional independence of covariate-specific outcome distribution $p(Y|X,T,t') = p(Y|X,T)$ and $p(Y_{t'}|X,t',T) = p(Y_{t'}|X,t')$. Hence, the same proof for Theorem 1 applies to Corollary 2 by replacing T' with t' and Y' with $Y_{t'}$. □

I.2 Disentangled Exogenous Noise Abduction

I.2.1 Proof of Lemma 1

Proof. Let $S_I = Z$ and $S_{\setminus I} = T$. On one hand,

$$\begin{aligned}
&\mathbb{E}_{p_0,p^*}\|\tilde{q}_I \circ p^*((s_I, s_{\setminus I}); x) - \tilde{q}_I \circ p^*((s_I, s'_{\setminus I}); x)\| \\
&= \mathbb{E}_{p_0(x),p_0(s_I,s_{\setminus I},s'_{\setminus I}|x),p_0(v|s_I,s_{\setminus I}),p_0(v'|s_I,s'_{\setminus I})}\|\tilde{q}_I(v,x) - \tilde{q}_I(v',x)\| && (40)\\
&= \mathbb{E}_{p_0(x)p_0(z,t,t'|x),p_0(y|z,t),p_0(y'|z,t')}\|\tilde{q}_I(y,t,x) - \tilde{q}_I(y',t',x)\| && (41)\\
&= \mathbb{E}_{p_0(x,t,t',y,y')}\|q(Z|y,t,x) - q(Z|y',t',x)\| && (42)\\
&\leq \mathbb{E}_{p_0(d)} D_{\mathrm{KL}}\left[q(Z|y,t,x) \parallel q(Z|y',t',x)\right] \quad \text{(Pinsker's inequality)} && (43)\\
&= 0, && (44)
\end{aligned}$$

hence $\tilde{q}$ is consistent with Z. On the other hand, $\tilde{q}$ is restricted to Z by design:

$$\begin{aligned}
&\mathbb{E}_{p_0,p*}\|\tilde{q}_{\setminus I} \circ p^*((s_I, s_{\setminus I}); x) - \tilde{q}_{\setminus I} \circ p^*((s'_I, s_{\setminus I}); x)\| \\
&= \mathbb{E}_{p_0(s_I,s'_I,s_{\setminus I},x),p_0(v|s_I,s_{\setminus I}),p_0(v'|s'_I,s_{\setminus I})}\|\tilde{q}_{\setminus I}(v,x) - \tilde{q}_{\setminus I}(v',x)\| && (45)\\
&= \mathbb{E}_{p_0(z,z',t,x),p_0(y|z,t),p_0(y'|z',t)}\|\tilde{q}_{\setminus I}(y,t,x) - \tilde{q}_{\setminus I}(y',t,x)\| && (46)\\
&= \mathbb{E}_{p_0(t)}\|\delta_t(T) - \delta_t(T)\| && (47)\\
&= 0. && (48)
\end{aligned}$$

Therefore $\tilde{q}$ disentangles Z and T. □

I.2.2 Proof of Proposition 1

Assumption 3 (Uniqueness)**.** *Two different individuals do not have the exact same outcome (a.s.) under the same treatment α, i.e. for $y \sim p(Y|z,\alpha)$, $y' \sim p(Y|z',\alpha)$, we have $y \neq y'$ a.s. if $z \neq z'$.*

The uniqueness assumption is weak and automatically satisfied under common assumptions in prior works such as injective decoder, continuous outcome or diffeomorphism (Khemakhem et al., 2020; von Kügelgen et al., 2023). Note that this assumption is unrealistic in traditional causal inference but completely reasonable in high-dimensional outcome settings. Take facial imaging dataset for example, no two individuals with different facial features should look exactly identical pixel-by-pixel under the same treatment.

Proof. Denote

$$\begin{aligned}
LB(p_\cdot, q_\cdot) := \mathbb{E}_{p_0(d)}\{&\mathbb{E}_{q_\cdot(z|y,t,x)} \log\left[p_\cdot(y|z,t)\right] + \log\left[\hat{p}(y'|x,t')\right] \\
&- D_{\mathrm{KL}}\left[q_\cdot(Z|y,t,x) \parallel q_\cdot(Z|y',t',x)\right]\}
\end{aligned} \tag{49}$$

and suppose that $(p_*, q_*) \in \arg\max_{p_\cdot,q_\cdot} LB(p_\cdot, q_\cdot)$ but

$$\mathbb{E}_{p_0(d)} D_{\mathrm{KL}}\left[q_*(Z|y,t,x) \parallel q_*(Z|y',t',x)\right] > 0, \tag{50}$$

which we can factorize as

$$\mathbb{E}_{p_0(x,z,t,t'),p^*} D_{\mathrm{KL}}\left[q_* \circ p^*(z,t;x) \parallel q_* \circ p^*(z,t';x)\right] > 0 \tag{51}$$

where $p^*(z,t) = (p_0(Y|z,t), \delta_t(T))$. Then we consider model (p_{**}, q_{**}) such that $\forall x,z,t$, we have

$$q_{**}(Z|f_0(z,t,0),t,x) = \delta_{\gamma(z)}(Z) \tag{52}$$

$$p_{**}(Y|\gamma(z),t) = \delta_{f_0(z,t,0)}(Y) \tag{53}$$

where $f_0(z, t, \epsilon_Y) = p_0(Y|z, t)$ is the true SCM and γ is any injective transformation of z (e.g. $\gamma(z) = z$). Equation 52 is well-defined by Assumption 2 and 3, which guarantees that $f_0(z, t, 0) \neq f_0(z', t, 0)$ for $z \neq z'$; Equation 53 is well-defined due to the injectiveness of γ. $q_{**} = q_*$, $p_{**} = p_*$ elsewhere. It follows that

$$\begin{aligned}
&\mathbb{E}_{p_0(d)} D_{\mathrm{KL}} \left[q_{**}(Z|y, t, x) \parallel q_{**}(Z|y', t', x) \right] \\
&= \mathbb{E}_{p_0(x,z,t,t'),p^*} D_{\mathrm{KL}} \left[q_* \circ p^*(z, t; x) \parallel q_* \circ p^*(z, t'; x) \right] && (54) \\
&= \mathbb{E}_{p_0(x,z,t,t')} D_{\mathrm{KL}} \left[q_{**}(Z|f_0(z, t, 0), t, x) \parallel q_{**}(Z|f_0(z, t', 0), t', x) \right] && (55) \\
&= \mathbb{E}_{p_0(x,z,t,t')} D_{\mathrm{KL}} \left[\delta_{\gamma(z)}(Z) \parallel \delta_{\gamma(z)}(Z) \right] && (56) \\
&< \mathbb{E}_{p_0(d)} D_{\mathrm{KL}} \left[q_*(Z|y, t, x) \parallel q_*(Z|y', t', x) \right] && (57)
\end{aligned}$$

by Assumption 2, in the meantime

$$\begin{aligned}
&\mathbb{E}_{p_0(d)} \mathbb{E}_{q_{**}(z|y,t,x)} \log \left[p_{**}(y|z, t) \right] \\
&= \mathbb{E}_{p_0(x,z,t),p_0(y|z,t)} \mathbb{E}_{q_{**}(z_{**}|y,t,x)} \log \left[p_{**}(y|z_{**}, t) \right] && (58) \\
&= \mathbb{E}_{p_0(x,z,t)} \mathbb{E}_{q_{**}(z_{**}|f_0(z,t,0),x,t)} \log \left[p_{**}(f_0(z, t, 0)|z_{**}, t) \right] && (59) \\
&= \mathbb{E}_{p_0(x,z,t)} \log \left[p_{**}(f_0(z, t, 0)|\gamma(z), t) \right] && (60) \\
&= \mathbb{E}_{p_0(x,z,t)} \log \left[\delta_{f_0(z,t,0)}(f_0(z, t, 0)) \right] && (61) \\
&= \mathbb{E}_{p_0(x,z,t)} \mathbb{E}_{q_*(z_*|f_0(z,t,0),x,t)} \log \left[\delta_{f_0(z,t,0)}(f_0(z, t, 0)) \right] && (62) \\
&\geq \mathbb{E}_{p_0(x,z,t)} \mathbb{E}_{q_*(z_*|f_0(z,t,0),x,t)} \log \left[p_*(y|z_*, t) \right] && (63) \\
&= \mathbb{E}_{p_0(x,z,t),p_0(y|z,t)} \mathbb{E}_{q_*(z_*|y,t,x)} \log \left[p_*(y|z_*, t) \right] && (64) \\
&= \mathbb{E}_{p_0(d)} \mathbb{E}_{q_*(z|y,t,x)} \log \left[p_*(y|z, t) \right] && (65)
\end{aligned}$$

by Assumption 2. Hence we have

$$LB(p_{**}, q_{**}) > LB(p_*, q_*) \tag{66}$$

which contradicts $(p_*, q_*) \in \arg\max_{p_{\cdot}, q_{\cdot}} LB(p_{\cdot}, q_{\cdot})$. Therefore (p_*, q_*) must satisfy

$$\mathbb{E}_{p_0(d)} D_{\mathrm{KL}} \left[q_*(Z|y, t, x) \parallel q_*(Z|y', t', x) \right] = 0 \tag{67}$$

and it follows that $\tilde{q}_*$ disentangles Z and T by Lemma 1. □

I.2.3 Proof of Proposition 2

Proof. The strategy is similar to the proof of Proposition 1. We first prove a statement similar to Lemma 1 that states a sufficient condition for empirical disentanglement (**sufficiency**), and then argue that this condition is attainable by optimizing $J_{p_{\mathrm{data}}}(p_{\cdot}, q_{\cdot})$ (**attainability**).

Sufficiency We prove that if

$$\mathbb{E}_{p_{\mathrm{data}}(x,t,y),p_{\mathrm{data}}(t'|x),p_{\mathrm{data}}(t''|x)} D_{\mathrm{KL}} \left[q(Z|y'_{\cdot}, t', x) \parallel q(Z|y''_{\cdot}, t'', x) \right] = 0 \tag{68}$$

where $y'_{\cdot} = \mathbb{E}_{p_{\cdot}(Y|\mathbb{E}_{q(Z|y,t,x)}Z,t')} Y$ and $y''_{\cdot} = \mathbb{E}_{p_{\cdot}(Y|\mathbb{E}_{q(Z|y,t,x)}Z,t'')} Y$, then $(\tilde{g}_{\cdot}, \tilde{q})$ disentangles Z and T under $p_e = \int_y e \cdot p_{\mathrm{data}}$.

Let $S_I = Z$ and $S_{\setminus I} = T$. On one hand, notice that for any x, z s.t. $p_e(x, z) > 0$, we have $p_e(t|x, z) > 0$ only if $p_e(x, z, t) > 0$ only if $p_e(x, t) > 0$ only if $p_{\mathrm{data}}(x, t) > 0$ only if $p_{\mathrm{data}}(t|x) > 0$ for any t. It follows that

$$\begin{aligned}
&\mathbb{E}_{p_e,\tilde{g}_{\cdot}} \|\tilde{q}_I \circ \tilde{g}_{\cdot}(z, t'; x) - \tilde{q}_I \circ \tilde{g}_{\cdot}(z, t''; x)\| \\
&= \mathbb{E}_{p_{\mathrm{data}}(x,t,y),e(z|x,t,y),p_e(t',t''|x,z),\tilde{g}_{\cdot}} \|\tilde{q}_I \circ \tilde{g}_{\cdot}(z, t'; x) - \tilde{q}_I \circ \tilde{g}_{\cdot}(z, t''; x)\| && (69) \\
&= \mathbb{E}_{p_{\mathrm{data}}(x,t,y),p_e(t',t''|x,\mathbb{E}_{q(Z|y,t,x)}Z)} \|\tilde{q}_I(y'_{\cdot}, t', x) - \tilde{q}_I(y''_{\cdot}, t'', x)\| && (70) \\
&= \mathbb{E}_{p_{\mathrm{data}}(x,t,y),p_e(t',t''|x,\mathbb{E}_{q(Z|y,t,x)}Z)} \|q(Z|y'_{\cdot}, t', x) - q(Z|y''_{\cdot}, t'', x)\| && (71) \\
&\leq \mathbb{E}_{p_{\mathrm{data}},p_e} D_{\mathrm{KL}} \left[q(Z|y'_{\cdot}, t', x) \parallel q(Z|y''_{\cdot}, t'', x) \right] \quad \text{(Pinsker's inequality)} && (72) \\
&= 0, && (73)
\end{aligned}$$

since Equation 68 implies that $D_{\mathrm{KL}}[q(Z|y'_\cdot, t', x) \parallel q(Z|y''_\cdot, t'', x)] = 0$ for any x, t, y, t', t'' s.t. $p_{\mathrm{data}}(x,t,y) \cdot p_{\mathrm{data}}(t'|x) \cdot p_{\mathrm{data}}(t''|x) > 0$. Hence $(\tilde{g}_\cdot, \tilde{q})$ is consistent with Z under p_e. On the other hand, $(\tilde{g}_\cdot, \tilde{q})$ is restricted to Z under p_e by design:

$$\begin{aligned}
&\mathbb{E}_{p_e, \tilde{g}_\cdot} \|\tilde{q}_{\setminus I} \circ \tilde{g}_\cdot(z', t; x) - \tilde{q}_{\setminus I} \circ \tilde{g}_\cdot(z'', t; x)\| \\
&= \mathbb{E}_{p_e(x,t), p_e(z', z''|x,t), \tilde{g}_\cdot} \|\tilde{q}_{\setminus I} \circ \tilde{g}_\cdot(z', t; x) - \tilde{q}_{\setminus I} \circ \tilde{g}_\cdot(z'', t; x)\| && (74)\\
&= \mathbb{E}_{p_e(x,t), p_e(z', z''|x,t)} \|\tilde{q}_{\setminus I}(\mathbb{E}_{p_\cdot(Y|z',t)} Y, t, x) - \tilde{q}_{\setminus I}(\mathbb{E}_{p_\cdot(Y|z'',t)} Y, t, x)\| && (75)\\
&= \mathbb{E}_p \|\delta_t(T) - \delta_t(T)\| && (76)\\
&= 0. && (77)
\end{aligned}$$

Therefore $(\tilde{g}_\cdot, \tilde{q})$ disentangles Z and T under $\int_y e \cdot p_{\mathrm{data}}$.

Attainability Let $A = \{(x_{k_i}, t_{k_i}, y_{k_i})\}|_{i=1}^m$ be the set of all unique entries in $\{(x_k, t_k, y_k)\}|_{k=1}^n$. Suppose that $(p_*, q_*) \in \arg\max_{p_\cdot, q_\cdot} J_{p_{\mathrm{data}}}(p_\cdot, q_\cdot)$ but

$$\mathbb{E}_{p_{\mathrm{data}}(x,t,y), p_{\mathrm{data}}(t'|x), p_{\mathrm{data}}(t''|x)} D_{\mathrm{KL}}\left[q_*(Z|y'_*, t', x) \parallel q_*(Z|y''_*, t'', x)\right] > 0, \tag{78}$$

where $y'_* = \mathbb{E}_{p_*(Y|\mathbb{E}_{q_*(Z|y,t,x)}Z, t')} Y$ and $y''_* = \mathbb{E}_{p_*(Y|\mathbb{E}_{q_*(Z|y,t,x)}Z, t'')} Y$, i.e. $\exists l : 1 \le l \le n$ and $\exists t^{(1)}, t^{(2)} : p_{\mathrm{data}}(t^{(1)}|x_l) \cdot p_{\mathrm{data}}(t^{(2)}|x_l) > 0$ such that

$$D_{\mathrm{KL}}\left[q(Z|y_*^{(1)}, t^{(1)}, x_l) \parallel q(Z|y_*^{(2)}, t^{(2)}, x_l)\right] > 0 \tag{79}$$

where $y_*^{(1)} = \mathbb{E}_{p_*(Y|\mathbb{E}_{q_*(Z|y_l,t_l,x_l)}Z, t^{(1)})} Y$ and $y_*^{(2)} = \mathbb{E}_{p_*(Y|\mathbb{E}_{q_*(Z|y_l,t_l,x_l)}Z, t^{(2)})} Y$. Then we consider model (p_{**}, q_{**}) such that $\forall (x,t,y) \in A$, we have

$$q_{**}(Z|\mathbb{E}_{p_*(Y|\mathbb{E}_{q_*(Z|y,t,x)}Z, \alpha)} Y, \alpha, x) = q_*(Z|y, t, x) \tag{80}$$

for any α s.t. $p_{\mathrm{data}}(T = \alpha|x) > 0$. Equation 80 is well-defined since

$$\begin{aligned}
&\mathbb{E}_{p_*(Y|\mathbb{E}_{q_*(Z|y,t,x)}Z, \alpha)} Y = \mathbb{E}_{p_*(Y|\mathbb{E}_{q_*(Z|y',t',x)}Z, \alpha)} Y \\
\Leftrightarrow\ & g_*(Y|\mathbb{E}_{q_*(Z|y,t,x)}Z, \alpha) = g_*(Y|\mathbb{E}_{q_*(Z|y',t',x)}Z, \alpha) \Rightarrow \mathbb{E}_{q_*(Z|y,t,x)}Z = \mathbb{E}_{q_*(Z|y',t',x)}Z && (81)\\
\Leftrightarrow\ & e_*(Z|y,t,x) = e_*(Z|y',t',x) \Rightarrow (y,t) = (y',t') \Rightarrow q_*(Z|y,t,x) = q_*(Z|y',t',x) && (82)
\end{aligned}$$

by uniqueness condition 1) and the construction of $\{q_\cdot\}$. $q_{**} = q_*$ elsewhere and $p_{**} = p_*$ everywhere.

Firstly, we show that (p_{**}, q_{**}) is still a member of the model class of interest. Since q_{**} is still normally distributed with unit variance by definition and g_{**} still satisfies uniqueness condition 1) by definition, we only need to show that (g_{**}, e_{**}) still satisfies uniqueness condition 2). This is because $\forall x,t,y,t' : p_{\mathrm{data}}(x,t,y) \cdot p_{\mathrm{data}}(t'|x) > 0$, we have $(x,t,y) \in A$ and thus $(x,t,y) = (x, \alpha, \mathbb{E}_{p_*(Y|\mathbb{E}_{q_*(Z|y_{k_i},t_{k_i},x_{k_i})}Z, \alpha)} Y)$ for some $(x_{k_i}, t_{k_i}, y_{k_i}) \in A$ only if

$$(x, \alpha, \mathbb{E}_{p_*(Y|\mathbb{E}_{q_*(Z|y_{k_i},t_{k_i},x_{k_i})}Z, \alpha)} Y) = (x, \alpha, \mathbb{E}_{g_*(Y|z,t')e_*(z|y_{k_i},t_{k_i},x_{k_i})} Y) \in A \tag{83}$$

only if $(x, \alpha, \mathbb{E}_{p_*(Y|\mathbb{E}_{q_*(Z|y_{k_i},t_{k_i},x_{k_i})}Z, \alpha)} Y) = (x_{k_i}, t_{k_i}, y_{k_i})$ by the fact that (g_*, e_*) satisfies uniqueness condition 2). In this case, we have $(x,t,y) = (x_{k_i}, t_{k_i}, y_{k_i})$ and

$$\begin{aligned}
q_{**}(Z|y,t,x) &= q_{**}(Z|\mathbb{E}_{p_*(Y|\mathbb{E}_{q_*(Z|y_{k_i},t_{k_i},x_{k_i})}Z, \alpha)} Y, \alpha, x) && (84)\\
&= q_*(Z|y_{k_i}, t_{k_i}, x_{k_i}) = q_*(Z|y,t,x). && (85)
\end{aligned}$$

If $(x,t,y) \neq (x, \alpha, \mathbb{E}_{p_*(Y|\mathbb{E}_{q_*(Z|y_{k_i},t_{k_i},x_{k_i})}Z, \alpha)} Y)$ for any $(x_{k_i}, t_{k_i}, y_{k_i}) \in A$, then $q_{**}(Z|y,t,x) = q_*(Z|y,t,x)$ by definition. Therefore we have $q_{**}(Z|y,t,x) = q_*(Z|y,t,x)$. It follows that $y'_{**} = \mathbb{E}_{g_{**}(Y|z,t')e_{**}(z|y,t,x)} Y = \mathbb{E}_{g_*(Y|z,t')e_*(z|y,t,x)} Y = y'_*$ and (g_{**}, e_{**}) satisfies uniqueness condition 2) by the fact that (g_*, e_*) satisfies uniqueness condition 2).

Secondly, we show that (p_*, q_*) is no longer optimal, thus raise a contradiction. On one hand, we must have

$$\mathbb{E}_{p_{\mathrm{data}}} D_{\mathrm{KL}}\left[q_*(Z|y,t,x) \parallel q_*(Z|y'_*, t', x)\right]$$

$$\geq p_{\text{data}}(x_l, t_l, y_l) \Big\{ p_{\text{data}}(t^{(1)}|x_l) D_{\text{KL}} \left[q_*(Z|y_l, t_l, x_l) \parallel q_*(Z|y_*^{(1)}, t^{(1)}, x_l) \right] + p_{\text{data}}(t^{(2)}|x_l) D_{\text{KL}} \left[q_*(Z|y_l, t_l, x_l) \parallel q_*(Z|y_*^{(2)}, t^{(2)}, x_l) \right] \Big\} \tag{86}$$

$$> 0, \tag{87}$$

otherwise we would have $q_*(Z|y_l, t_l, x_l) = q_*(Z|y_*^{(1)}, t^{(1)}, x_l) = q_*(Z|y_*^{(2)}, t^{(2)}, x_l)$ a.e. which contradicts Equation 79. Hence

$$\begin{aligned}
&\mathbb{E}_{p_{\text{data}}} D_{\text{KL}} \left[q_{**}(Z|y, t, x) \parallel q_{**}(Z|y'_{**}, t', x) \right] \\
&= \sum_{(x,t,y) \in A} p_{\text{data}}(x, t, y) \sum_{t'} p_{\text{data}}(t'|x) \cdot D_{\text{KL}} \left[q_*(Z|y, t, x) \parallel q_{**}(Z|y'_{**}, t', x) \right] &(88)\\
&= \sum_{(x,t,y) \in A} p_{\text{data}}(x, t, y) \sum_{t'} p_{\text{data}}(t'|x) \cdot D_{\text{KL}} \left[q_*(Z|y, t, x) \parallel q_*(Z|y, t, x) \right] &(89)\\
&= 0 < \mathbb{E}_{p_{\text{data}}} D_{\text{KL}} \left[q_*(Z|y, t, x) \parallel q_*(Z|y'_*, t', x) \right] &(90)
\end{aligned}$$

by Equation 80 and the fact that $q_{**}(Z|y, t, x) = q_*(Z|y, t, x)$ for any $(x, t, y) \in A$ as shown above. On the other hand, we have

$$\begin{aligned}
&\mathbb{E}_{p_{\text{data}}} \left\{ \mathbb{E}_{q_{**}(z|y,t,x)} \log \left[p_{**}(y|z, t) \right] + \log \left[\hat{p}(y'_{**}|x, t') \right] \right\} \\
&= \mathbb{E}_{p_{\text{data}}} \left\{ \mathbb{E}_{q_*(z|y,t,x)} \log \left[p_*(y|z, t) \right] + \log \left[\hat{p}(y'_*|x, t') \right] \right\} &(91)
\end{aligned}$$

simply by the construction of p_{**} and the fact that $q_{**}(Z|y, t, x) = q_*(Z|y, t, x)$, $y'_{**} = y'_*$ for any $(x, t, y) \in A$ as shown above. Hence we have

$$J_{p_{\text{data}}}(p_{**}, q_{**}) > J_{p_{\text{data}}}(p_*, q_*) \tag{92}$$

which contradicts $(p_*, q_*) \in \arg\max_{p_\cdot, q_\cdot} J_{p_{\text{data}}}(p_\cdot, q_\cdot)$. Therefore (p_*, q_*) must satisfy

$$\mathbb{E}_{p_{\text{data}}(x,t,y), p_{\text{data}}(t'|x), p_{\text{data}}(t''|x)} D_{\text{KL}} \left[q_*(Z|y'_*, t', x) \parallel q_*(Z|y''_*, t'', x) \right] = 0 \tag{93}$$

and it follows that $(\tilde{g}_*, \tilde{q}_*)$ disentangles Z and T under $\int_y e_* p_{\text{data}}$ by **sufficiency**. □

I.2.4 Proof of Corollary 1

Proof. By the proof of Proposition 2 (attainability), we have

$$\mathbb{E}_{p_{\text{data}}(x,t,y), p_{\text{data}}(t'|x), p_{\text{data}}(t''|x)} D_{\text{KL}} \left[q_*(Z|y'_*, t', x) \parallel q_*(Z|y''_*, t'', x) \right] = 0 \tag{94}$$

where $y'_* = \mathbb{E}_{p_*(Y|\mathbb{E}_{q_*(Z|y,t,x)} Z, t')} Y$ and $y''_* = \mathbb{E}_{p_*(Y|\mathbb{E}_{q_*(Z|y,t,x)} Z, t'')} Y$, hence $\mathbb{E}_{q_*(Z|y'_*, t', x)} Z = \mathbb{E}_{q_*(Z|y''_*, t'', x)} Z$ a.e. on p_{data} and it follows that

$$\begin{aligned}
&\mathbb{E}_{p_{\text{data}}(x,t,y), p_{\text{data}}(t'|x), p_{\text{data}}(t''|x)} D_{\text{KL}} \left[e_*(Z|y'_*, t', x) \parallel e_*(Z|y''_*, t'', x) \right] \\
&= \mathbb{E}_{p_{\text{data}}(x,t,y), p_{\text{data}}(t'|x), p_{\text{data}}(t''|x)} D_{\text{KL}} \left[\delta_{\mathbb{E}_{q_*(Z|y'_*, t', x)} Z} \parallel \delta_{\mathbb{E}_{q_*(Z|y''_*, t'', x)} Z} \right] = 0. &(95)
\end{aligned}$$

Notice that $y'_* = \mathbb{E}_{p_*(Y|\mathbb{E}_{e_*(Z|y,t,x)} Z, t')} Y$ and $y''_* = \mathbb{E}_{p_*(Y|\mathbb{E}_{e_*(Z|y,t,x)} Z, t'')} Y$, we have $(\tilde{g}_*, \tilde{e}_*)$ disentangles Z and T under $\int_y e_* p_{\text{data}}$ by the proof of Proposition 2 (sufficiency). □

I.3 Marginal Estimator

I.3.1 Proof of Theorem 2

Proof. $\Psi(p)$ has the identification $\Psi(p) = \mathbb{E}_p[\mathbb{E}_p[Y'|Z, X, T' = \alpha]] = \mathbb{E}_p[\mathbb{E}_p[Y'|Z, T' = \alpha]]$ under Figure 1. Following Van der Vaart (2000), we define a path $p_\epsilon(\Lambda) = p(\Lambda)(1 + \epsilon S(\Lambda))$ on density p of random vector Λ as a submodel that passes through p at $\epsilon = 0$ in the direction of the score $S(\Lambda) = \frac{d}{d\epsilon} \log[p_\epsilon(\Lambda)] \Big|_{\epsilon=0}$. Following the key identity presented in Levy (2019):

$$\frac{d}{d\epsilon} p_\epsilon(\lambda_i | pa(\Lambda_i) = \bar{\lambda}_{i-1}) \Big|_{\epsilon=0}$$

$$= p(\lambda_i | pa(\Lambda_i) = \bar{\lambda}_{i-1})(\mathbb{E}[S(\Lambda)|\Lambda_i = \lambda_i, pa(\Lambda_i) = \bar{\lambda}_{i-1}] - \mathbb{E}[S(\Lambda)|pa(\Lambda_i) = \bar{\lambda}_{i-1}]) \tag{96}$$

where $pa(\Lambda_i)$ denotes the parent nodes of variable Λ_i, we have

$$\begin{aligned}
\frac{d}{d\epsilon}\Psi(p_\epsilon)\Big|_{\epsilon=0} &= \frac{d}{d\epsilon}\Big|_{\epsilon=0}\mathbb{E}_{p_\epsilon}\left[\mathbb{E}_{p_\epsilon}\left[Y'|Z, T'=\alpha\right]\right] && (97)\\
&= \frac{d}{d\epsilon}\Big|_{\epsilon=0}\int_{y',z,x} y'\left[p_\epsilon(y'|z,T'=\alpha)p_\epsilon(z,x)\right] && (98)\\
&= \int_{y',z,x} y'\frac{d}{d\epsilon}\Big|_{\epsilon=0}\left[p_\epsilon(y'|z,T'=\alpha)p_\epsilon(z,x)\right] \quad \text{(dominated convergence)} && (99)\\
&= \int_{y',z,x} y'p(z,x)\frac{d}{d\epsilon}\Big|_{\epsilon=0}p_\epsilon(y'|z,T'=\alpha) && (100)\\
&+ \int_{y',z,x} y'p(y'|z,T'=\alpha)\frac{d}{d\epsilon}\Big|_{\epsilon=0}p_\epsilon(z,x) && (101)\\
&= \int_w I(t'=\alpha)\frac{p(t'|x)}{p(t'|x)}y'p(y,t|z,x)p(z,x)\frac{d}{d\epsilon}\Big|_{\epsilon=0}p_\epsilon(y'|z,t')\\
&\quad + \int_{y',z,x} y'p(y'|z,T'=\alpha)\frac{d}{d\epsilon}\Big|_{\epsilon=0}p_\epsilon(z,x) && (102)\\
&= \int_w \frac{I(t'=a)}{p(t'|x)}y'p(y',t'|z,x)p(y,t|z,x)p(z,x)\left\{S(w) - \mathbb{E}\left[S(W)|y,z,x,t,t'\right]\right\}\\
&\quad + \int_{y',z,x} y'p(y'|z,T'=\alpha)p(z,x)\left\{\mathbb{E}\left[S(W)|z,x\right] - \mathbb{E}\left[S(W)\right]\right\} && (103)\\
&= \int_w \frac{I(t=a)}{p(t|x)}yp(y,t|z,x)p(y',t'|z,x)p(z,x)\left\{S(w) - \mathbb{E}\left[S(W)|y',z,x,t',t\right]\right\}\\
&\quad + \int_{y',z,x} y'p(y'|z,T'=\alpha)p(z,x)\left\{\mathbb{E}\left[S(W)|z,x\right] - \mathbb{E}\left[S(W)\right]\right\} && (104)\\
&= \int_w S(w)\cdot\frac{I(t=\alpha)}{p(t|x)}yp(w)\\
&\quad - \int_w \mathbb{E}\left[S(W)|y',z,x,t,t'\right]p(y',z,x,t,t')\cdot\frac{I(t=\alpha)}{p(t|x)}yp(y|z,t)\\
&\quad + \int_{y',z,x}\mathbb{E}\left[S(W)|z,x\right]p(z,x)\cdot y'p(y'|z,T'=\alpha)\\
&\quad - \int_{y',z,x}\mathbb{E}\left[S(W)\right]\cdot y'p(y'|z,T'=\alpha)p(z,x) && (105)\\
&= \int_w S(w)\left\{\frac{I(t=\alpha)}{p(t|x)}(y - \mathbb{E}\left[Y|z,t\right]) + \mathbb{E}\left[Y'|z,T'=\alpha\right] - \Psi\right\}p(w) && (106)
\end{aligned}$$

by the assumption of Theorem 2 and factorization according to Figure 1. Hence

$$\frac{d}{d\epsilon}\Psi(p_\epsilon)\Big|_{\epsilon=0} = \left\langle S(W), \frac{I(T=\alpha)}{p(T|X)}(Y - \mathbb{E}_p\left[Y|Z,T\right]) + \mathbb{E}_p\left[Y'|Z,T'=\alpha\right] - \Psi\right\rangle_{L^2(\Omega;E)} \tag{107}$$

and we have $\tilde{\psi}_p = I(T=\alpha)/p(T|X)\cdot(Y - \mathbb{E}_p[Y|Z,T]) + \mathbb{E}_p[Y'|Z,T'=\alpha] - \Psi$. □

I.3.2 Proof of Corollary 3

Proof. The proof is a simple extension on the proof of Theorem 2. We have

$$\begin{aligned}
\frac{d}{d\epsilon}\Xi(p_\epsilon)\Big|_{\epsilon=0} &= \frac{d}{d\epsilon}\Big|_{\epsilon=0}\mathbb{E}_{p_\epsilon}\left[\mathbb{E}_{p_\epsilon}\left[Y'|Z,T'=\alpha\right]|X=c\right] && (108)\\
&= \frac{d}{d\epsilon}\Big|_{\epsilon=0}\int_{y',z,x} y'\left[p_\epsilon(y'|z,T'=\alpha)p_\epsilon(z|X=c)\right]. && (109)
\end{aligned}$$

Hence, following the same derivation, $p_\epsilon(z, x)$ in Equation 99 and onwards becomes $p_\epsilon(z|X = c)$, while $p(z, x)$ in Equation 102 and onwards becomes $I(x = c)/p(x) \cdot p(z, x)$. Therefore, we have $\tilde{\xi}_p(W) = I(X = c)/p(X) \cdot \tilde{\psi}_p(W)$. □

J Model Architecture for Image Generation Tasks

The specific model architecture used for image generation can be found in Figure 8. Note that in the image generation tasks in our experiments, we treated every condition as intervenable, thus every condition belongs in T rather than X. If this is not the case, the non-intervenable conditions would compose covariates X and would only be inputted to the encoding model but not the decoding model.

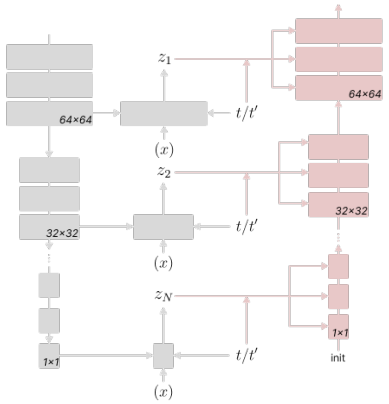

Figure 8: Model architecture of the latent recognition model (grey) and outcome construction model (pink) for image generation tasks.

To incorporate t (t') and x into the convolutional layers, we first embed them into vector representations (tabular embedding for categorical variables; sinusoidal embedding with non-linear mapping for continuous variable), then repeat and expand each value of the vectors to match the input resolutions of the corresponding blocks and concatenate them to image representations as extra channels, similar to Monteiro et al. (2023). Note that there are other ways to conduct image-vector incorporation such as the scale-shift approach commonly used in diffusion models to incorporate time step variable (Sanchez & Tsaftaris, 2022). Each convolutional block (each rectangle in Figure 8) contains a 1×1 embedding layer, a 3×3 (or 1×1 if resolution is lower than 3×3) botteleneck layer, and a 3×3 (or 1×1 if resolution is lower than 3×3) output layer.

K Detaching Patterns

In practice, there are a few optional gradient detaching options when evaluating the divergence term to enhance the stability of stochastic optimization. Our default behavior is to use a copy of q_ϕ for the evaluation of the divergence term which is updated after every epoch, while preserving the gradient path and gradient computation for $y'_{\theta,\phi}$. This technique is analogous to the handling of surrogate objectives commonly applied in reinforcement learning (Lillicrap et al., 2015; Van Hasselt et al., 2016; Schulman et al., 2017), and the copy of q_ϕ is seen as the target network. In addition, we provide the option of detaching ϕ from $y'_{\theta,\phi}$ (focusing on the second purpose described in divergence interpretation: preservation of individuality in decoding) and the option of not detaching the gradient computation for q_ϕ (reflecting the first purpose in divergence interpretation: recognition of mutual features in encoding) during the evaluation of the latent divergence term.

L Benchmark Adaptations

L.1 Autoencoder

The adapted autoencoder reconstructs the outcome during training similar to a generic autoencoder, but takes treatment and covariates as additional inputs. During test time, we simply plug in the

counterfactual treatments along with factual outcomes and covariates to generate the counterfactual outcome predictions.

L.2 GANITE

GANITE (Yoon et al., 2018)'s counterfactual generator does not scale with a combination of high-dimensional outcome and multi-level treatment, thus here we only input one randomly sampled counterfactual treatment to the generator and correspondingly construct one counterfactual outcome for each sample. See Figure 9 for the original and adapted structure of the model.

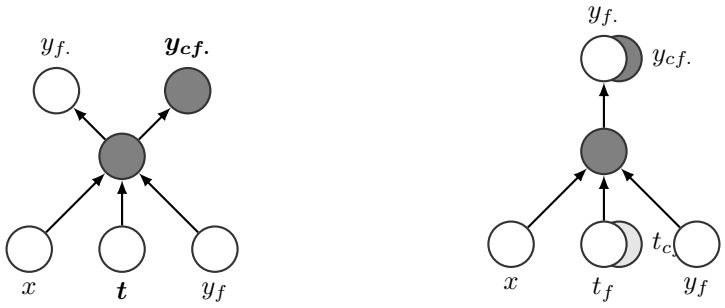

(a) original (b) adapted

Figure 9: GANITE's counterfactual generator. t_{cf} is a random sample of $\boldsymbol{t}$, passed into the generator as a part of the input (x, t_{cf}, y_f), separately from input (x, t_f, y_f) of the factual generation.

The discriminator predicts the logits l_f, l_{cf} of y_f, $y_{cf.}$ separately. The cross entropy loss of (l_f, l_{cf}) against $(1, 0)$ is then calculated.

M Discussion on Composition, Effectiveness, and Reversibility

Due to the popularity of the recently proposed composition, effectiveness and reversibility metrics (Monteiro et al., 2023), we feel the necessity to include a discussion here dive specifically into their purpose and use case, as well as why we did not use them for the evaluation of Morpho-MNIST. We clarify that we do think composition, effectiveness and reversibility are great evaluation metrics for most real-world datasets, however, it is very important to note that composition, effectiveness and reversibility are metrics developed in service for the scenario where *counterfactual truths are not attainable* (Monteiro et al., 2023), which is often the case for real-world datasets, to indirectly assess models' counterfactual generative capability through axiomatic soundness. However, Morpho-MNIST is a dataset where *counterfactual truths are attainable* and can be directly computed for hand-written digits, hence direct error measurements for the counterfactual generations against the counterfactual truths can be calculated, as shown in Table 2.

Readers with more experience in this field might quickly notice that, these three metrics almost mirror the three terms in our variational lower bound (Equation 3) and without further assumptions, there is generally a clear trade-off relation among them: for example, if one establishes a naive model that simply returns the input factual outcome as the counterfactual construction, with the latent representation being any bijection of the input (i.e., $\text{encoder}(y, t, t', x) = \eta(y)$, $\text{decoder}(z, t, t', x) = \eta^{-1}(z)$), it will achieve the best possible evaluation scores on two of these three metrics (composition and reversibility), while doing poorly on effectiveness (corresponding to setting coefficient $(1, 0, 1)$ on the three terms of Equation 3); on the other hand, if a model simply returns the population's average outcome under intervention as counterfactual construction, it will achieve the best effectiveness score while doing poorly on composition and reversibility (corresponding to setting coefficient $(0, 1, 0)$ on the three terms of Equation 3). These are two common fail cases for counterfactual generative models, and needless to say, none of the models in these two examples are meaningful for the purpose of counterfactual generation, and the best counterfactual generative model or any reasonable counterfactual generative model will not achieve the best score on any of these three metrics if these two models (or models with similar properties) exist among benchmarks.

Despite these flaws, composition, effectiveness and reversibility are still great metrics to use for the purpose of model diagnosis on most real-world datasets, due to the simple fact that there has not been much better we could do in prior literature to truly numerically evaluate the quality of a model's counterfactual generations in the absence of counterfactual truths. In this paper, we particularly chose the Morpho-MNIST dataset as our primary image generation benchmark for numerical evaluations because, to the best of our knowledge, Morpho-MNIST is the only dataset among popular counterfactual generation benchmarks (Pendulum (Yang et al., 2021), Shadow-spotlight (Zhu et al., 2023), CelebA-HQ (Karras et al., 2017), UK-Biobank (Sudlow et al., 2015), etc.) where exogenous noise exist while counterfactual truths can also be computed. When the counterfactual truths are attainable, it barely makes any sense to use composition, effectiveness and reversibility instead of the direct measures of error between the counterfactual constructions and counterfactual truths to evaluate a model's counterfactual generation capability. Hence we, as well as Ribeiro et al. (2023) (the same group that previously proposed composition, effectiveness and reversibility), use exact error measures instead of composition, effectiveness and reversibility for the evaluations on Morpho-MNIST.

N Advancements upon Variational Causal Inference

Important advancements to Wu et al. (2022) have been made in this work and we summarize them as follows.

- Theorem 1 has been reformulated and reworked such that the objective is better motivated by high-dimensional counterfactual inference, and the counterfactual supervision term is more closely related to adversarial training.
- Lemma 1, Proposition 1, Proposition 2, Corollary 1 are proposed to shed more light on the theoretical properties of latent disentanglement; Definition 1, Definition 2, Definition 3, Assumption 2, Assumption 1 are proposed to strengthen the rigorousness of our formulation and statements; Corollary 2 is proposed to relate the formulation to the traditional SCM settings and notations; Proposition 3 is proposed to present an alternative sample-heavy approach for implicit counterfactual supervision.
- The method was only applicable to vector outcomes, but is now capable of handling image outcomes with a carefully designed hierarchical convolutional architecture (Appendix J), and more thoroughly tested on popular counterfactual generative modeling benchmarks such as MorphoMNIST and CelebA-HQ. These benchmarks allow us to present more in-depth evaluations and metrics in order to examine the effectiveness of our framework.
- A figure clearly illustrating the workflow of our stochastic optimization scheme has been made (Figure 2) and ablation studies of the two additional terms of our framework have been performed (Figure 3). The proposed method can be a lot more difficult to understand without these two components, because its mechanism is very fresh and different from VAE, so we made sure that the illustration was presented in a simple and intuitive manner.
- More discussions have been made regarding the proposed method's relations and differences to VAE (Appendix B) and the proposed method's relations and differences to traditional causal formulation (Appendix B). These are important discussions to help readers understand our contributions and validity.

O Experiment Settings

O.1 Single-cell Perturbation Datasets

For both datasets in our experiments, two thousand most variable genes were selected for training and testing. Marson has 2,000 dimensional outcomes, 3 categorical covariates (cell type, donor indicator, stimulation indicator) and 1 categorical treatment (target gene), Sciplex has 2,000 dimensional outcomes, 2 categorical covariates (cell type, replicate indicator) and 1 categorical treatment (used drug). Data with certain treatment-covariate combinations are held out as the out-of-distribution (OOD) set and the rest are split into training and validation set with a four-to-one ratio.

Out-of-Distribution Selections We randomly select a covariate category (e.g. a cell type) and hold out all cells in this category that received one of the twenty perturbations whose effects are the hardest to predict. We use these held-out data to compose the out-of-distribution (OOD) set. We computed the Euclidean distance between the pseudobulked gene expression of each perturbation against the rest of the dataset, and selected the twenty most distant ones as the hardest-to-predict perturbations. This is the same procedure carried out by Lotfollahi et al. (2021).

Differentially-Expressed Genes In order to evaluate the quality of the predictions on the genes that were substantially affected by the perturbations, we select sets of 50 differentially-expressed (DE) genes associated with each perturbation and separately evaluate model performance on these genes. This is the same procedure carried out by Lotfollahi et al. (2021).

Hyperparameter Settings All common hyperparameters of all models are set to the same as the defaults of CPA (Lotfollahi et al., 2021): an universal number of hidden dimensions 128; number of layers 6 (encoder 3, decoder 3); an universal learning rate 3^{-4}, weight decay rate 4^{-7}. Contrary to CPA, we use step-based learning rate decay instead of epoch-based learning rate decay, and decay step size is set to $400,000$ while decay rate remains the same at 0.1. Batch size is 64 for Marson and 128 for Sciplex. For more details regarding the hyperparameter settings of our framework, see our code repository in the supplementary material.

Other Details We used the empirical outcome distribution (with Gaussian kernel smoother) stratified by X and T to estimate the covariate-specific outcome model $p(Y|X,T)$. The fully-attached detaching pattern is applied where both $y'_{\theta,\phi}$ and q_ϕ are not detached when evaluating the divergence term. Models are trained on Amazon web services' accelerated computing EC2 instance G4dn which contains 2nd Generation Intel Xeon Scalable Processors (Cascade Lake P-8259CL) and up to 8 NVIDIA T4 Tensor Core GPUs.

O.2 MORPHO-MNIST

We used the original Morpho-MNIST training set for model training, and the original Morpho-MNIST testing set as the observed samples for model testing. The training and testing set have 28×28 dimensional outcomes, no covariates and 2 continuous treatments (thickness, intensity). Three different testing sets are counstructed based on the counterfactual treatment settings: only modifying thickness for $do(\text{th})$; only modifying intensity for $do(\text{in})$; randomly modifying thickness or intensity for mix. For each observed sample in the testing set, we randomly sample the amount of modification based on the range of the selected modification.

Data Augmentation For each image in the training set (28×28), we pad it by a margin of 4 pixels on each side (36×36), then randomly crop a 32×32 region. This is the same procedure carried out by Ribeiro et al. (2023).

Hyperparameter Settings The model width, depth and resolutions of our framework are set to the same as Ribeiro et al. (2023): number of channels for the hierarchical encoding blocks are set to $\{16, 32, 64, 128, 256\}$ with resolutions $\{32, 16, 8, 4, 1\}$ and number of blocks $\{4, 4, 4, 4, 4\}$; number of channels for the hierarchical decoding blocks are set to $\{256, 128, 64, 32, 16\}$ with resolutions $\{1, 4, 8, 16, 32\}$ and number of blocks $\{4, 4, 4, 4, 4\}$. Each block contains a bottleneck layer with one-forth the number of channels as the input/output number of channels. Training is conducted with a batch size of 32, an universal learning rate 1^{-4}, and weight decay rate 4^{-5}. Learning rate decays at epoch 100 and linearly decays to 0 at epoch 200. For more details regarding the hyperparameter settings of our framework, see our code repository in the supplementary material.

Other Details We used the adversarial training approach to estimate the covariate-specific outcome model $p(Y|X,T)$. The default detaching pattern (see Appendix K) is applied where a copy of q_ϕ is used as critic to evaluate the divergence term, and updated after every epoch. Models are trained on Amazon web services' accelerated computing EC2 instance G4dn which contains 2nd Generation Intel Xeon Scalable Processors (Cascade Lake P-8259CL) and up to 8 NVIDIA T4 Tensor Core GPUs.

O.3 CELEBA-HQ

The two factors of interest – smiling and glasses, are regarded as intervenable. Therefore, the training and testing set have $64\times64\times3$ dimensional outcomes, no covariates and 2 categorical treatments. The train-test split of the CelebA-HQ dataset is inherited from the original CelebA dataset.

Data Augmentation For each image, we crop the 128×128 center region, then randomly crop a 120×120 region within the center region. Afterwards, we resize this region to 64×64, and apply horizontal flip with probability 0.5. Note that data augmentation is applied to both training and testing set in this experiment, since we are sampling and empirically examining the counterfactual results and not evaluating any metric.

Hyperparameter Settings The model width and resolutions of our framework are set to the same as Monteiro et al. (2023): number of channels for the hierarchical encoding blocks are set to $\{32, 64, 128, 256, 512, 1024\}$ with resolutions $\{64, 32, 16, 8, 4, 1\}$; number of channels for the hierarchical decoding blocks are set to $\{1024, 512, 256, 128, 64, 32\}$ with resolutions $\{1, 4, 8, 16, 32, 64\}$. The number of blocks is set to $\{3, 12, 12, 6, 3, 3\}$ for the encoder and $\{3, 3, 6, 12, 12, 3\}$ for the decoder. This is chosen to be slightly more shallow than Monteiro et al. (2023) ($\{4, 12, 12, 8, 4, 4\}$ and $\{4, 4, 8, 12, 12, 4\}$). Each block contains a bottleneck layer with one-forth the number of channels as the input/output number of channels. Training is conducted with a batch size of 32. An universal learning rate 3^{-4}, and weight decay rate 4^{-7} are inherited from the experiments with single-cell perturbation datasets. Step size for learning rate decay is $400,000$ with decay rate 0.1. For more details regarding the hyperparameter settings of our framework, see our code repository in the supplementary material.

Other Details We used the adversarial training approach to estimate the covariate-specific outcome model $p(Y|X,T)$. The default detaching pattern (see Appendix K) is applied where a copy of q_ϕ is used as critic to evaluate the divergence term, and updated after every epoch. Models are trained on Amazon web services' accelerated computing EC2 instance P3 which contains high frequency Intel Xeon Scalable Processor (Broadwell E5-2686 v4) and up to 8 NVIDIA Tesla V100 GPUs, each pairing 5,120 CUDA Cores and 640 Tensor Cores.

P ADDITIONAL EXPERIMENTS AND DETAILS

P.1 MARGINAL ESTIMATIONS ON SINGLE-CELL PERTURBATION DATASETS

In this section, we use the same evaluation metric as Section 3.1, but compute each R^2 with the robust marginal estimator and compare the results to that of the empirical mean estimator. Note that on OOD set, the robust estimator reduces to empirical mean since no perturbation-covariates combination exist in validation set. Therefore, we compute the R^2 of the marginal estimators using samples from the training set against the true empirical average on the validation set in these experiments. In each run, we train a VCI model for individualized outcome predictions, and calculate the evaluation metric for each marginal estimator periodically during the course of training. Table 5 shows the results on Marson. Note that the goal of robust estimation is to produce less biased estimators with tighter confidence bounds, hence we reported the mean and standard error over five independent runs to reflect its effectiveness regarding this goal.

Table 5: Comparison of marginal estimators on Marson (Schmidt et al., 2022)

	All Genes		DE Genes	
Episode	mean	robust	mean	robust
40	0.9141 ± 0.0159	$\mathbf{0.9343 \pm 0.0080}$	0.7108 ± 0.0735	$\mathbf{0.9146 \pm 0.0305}$
80	0.9171 ± 0.0104	$\mathbf{0.9349 \pm 0.0068}$	0.7274 ± 0.0462	$\mathbf{0.9163 \pm 0.0254}$
120	0.9204 ± 0.0097	$\mathbf{0.9352 \pm 0.0063}$	0.7526 ± 0.0447	$\mathbf{0.9182 \pm 0.0229}$
160	$0.9157 \pm \mathbf{0.0043}$	$\mathbf{0.9355} \pm 0.0053$	0.7383 ± 0.0402	$\mathbf{0.9203 \pm 0.0199}$

As is shown in the table, the robust estimator provides a crucial adjustment to the empirical mean of model predictions especially on the hard-to-predict elements of high-dimensional vectors. Such estimation could be valuable in many contexts involving high-dimensional predictions where deep learning models might plateau at rather low ceilings.

P.2 More Complete Ablation Study

Note that the latent divergence term is essentially a regularization term to counterfactual supervision, as discussed in Section 2.2, hence it would not be meaningful to train VCI with the latent divergence term and without the counterfactual supervision term – it would just further worsen the training-inference disconnection problem described in Section 1 without any real benefit. However, we acknowledge that presenting this case would make the ablation study more complete, and therefore have made this inclusion (marked as HAE-A) in Figure 10. As expected, HAE-A is even worse than HAE.

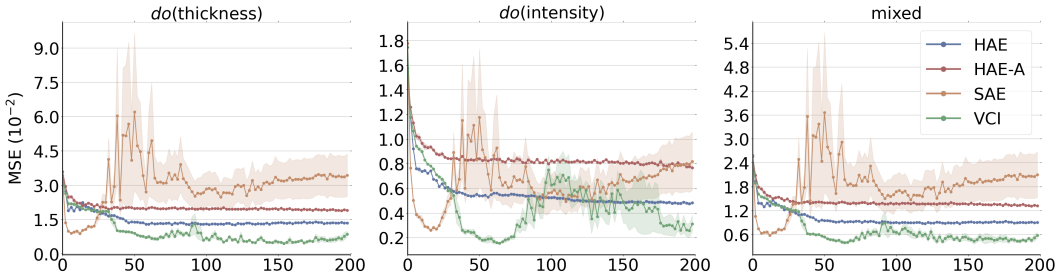

Figure 10: Ablation Study: Added HAE-A representing training VCI with the latent divergence term and without the counterfactual supervision term.

P.3 Disentanglement Evaluation on VCI's Exogenous Abduction

The definition of disentanglement (Definition 3) is extended from a well-established definition of disentanglement in Shu et al. (2019), based on the oracle consistency (Definition 1) of the latent representation. It is a different notion from latent disentanglement in the non-linear ICA literatures (Appendix A) although sometimes sharing a non-distinguishable terminology. So the best way to evaluate disentanglement in our context is by definition, using oracle consistency, and we present the ablation results in Table 6. As can be seen, a slight guidance from the exogenous disentanglement term can drastically improve the oracle consistency of Z.

Table 6: Oracle consistency under different strengths (denoted as coefficient ω_2) on the exogenous disentanglement term.

ω_2	oracle consistency ↓
0	3979.86 ± 202.42
0.01	0.84 ± 0.13
0.02	0.75 ± 0.11
0.03	0.53 ± 0.10
0.04	0.51 ± 0.07
0.05	0.51 ± 0.08

P.4 Composition, Effectiveness, and Reversibility

We compare ours with the best benchmark model in Table 2 on Composition, Effectiveness, and Reversibility. Note that these metrics are surrogate measurement of counterfactual models' axiomatic soundness served only as a reference – there is a trade-off between composition and effectiveness as well as effectiveness and reversibility, and it is inconclusive which of a pair of counterfactual models performs the best unless one model dominates the other on all three metrics (for example, as we

discussed in Appendix M, a model that simply returns the original image as counterfactual output will achieve a perfect composition score of 0 and a perfect reversibility score of 0).

Table 7: Composition, Effectiveness, and Reversibility of ours against the best benchmark model in Table 2. Images are scaled to $[0, 1]$ in evaluations. All losses are on the L-2 scale (note that the factors measured by effectiveness – thickness and intensity – are continuous values).

	β	composition ↓	effectiveness ↓	reversibility ↓
MED	1	0 ± 0	283.99 ± 67.76	0.01024 ± 0.00767
MED	3	0 ± 0	151.13 ± 86.46	0.00816 ± 0.00306
SAE		0.00048 ± 0.000084	189.03 ± 22.92	0.00102 ± 0.00019
VCI		0.00026 ± 0.000055	17.64 ± 6.23	0.00076 ± 0.00015

P.5 More Details on Morpho-MNIST Experiments

Table 8 shows the standard error of metrics reported in Table 2 across five independent runs. Figure 11 shows the violin plot of the errors reported in Table 2 and Table 8 across the corresponding runs. Figure 12 shows some sampled results from VCI.

Table 8: Standard error of metrics.

		Std. of Image MSE ($\cdot 10^{-2}$)			Std. of Thickness (th) MAE			Intensity (in) MAE ($\cdot 10^{-1}$)		
	β	do(th)	do(in)	mix	do(th)	do(in)	mix	do(th)	do(in)	mix
DEAR		0.20	0.06	0.11	0.18	0.10	0.21	0.32	0.49	0.25
CHVAE	1	0.53	0.86	0.62	0.03	0.15	0.10	0.33	0.32	0.20
CHVAE	3	0.90	0.83	0.94	0.04	0.21	0.08	0.19	0.10	0.17
MED	1	0.92	0.26	0.59	0.11	0.08	0.12	0.31	0.19	0.23
MED	3	1.34	0.40	0.86	0.05	0.06	0.07	0.25	0.09	0.15
SAE		0.12	0.05	0.05	0.10	0.04	0.05	0.15	0.10	0.08
VCI		0.07	0.01	0.07	0.03	0.01	0.05	0.11	0.05	0.06

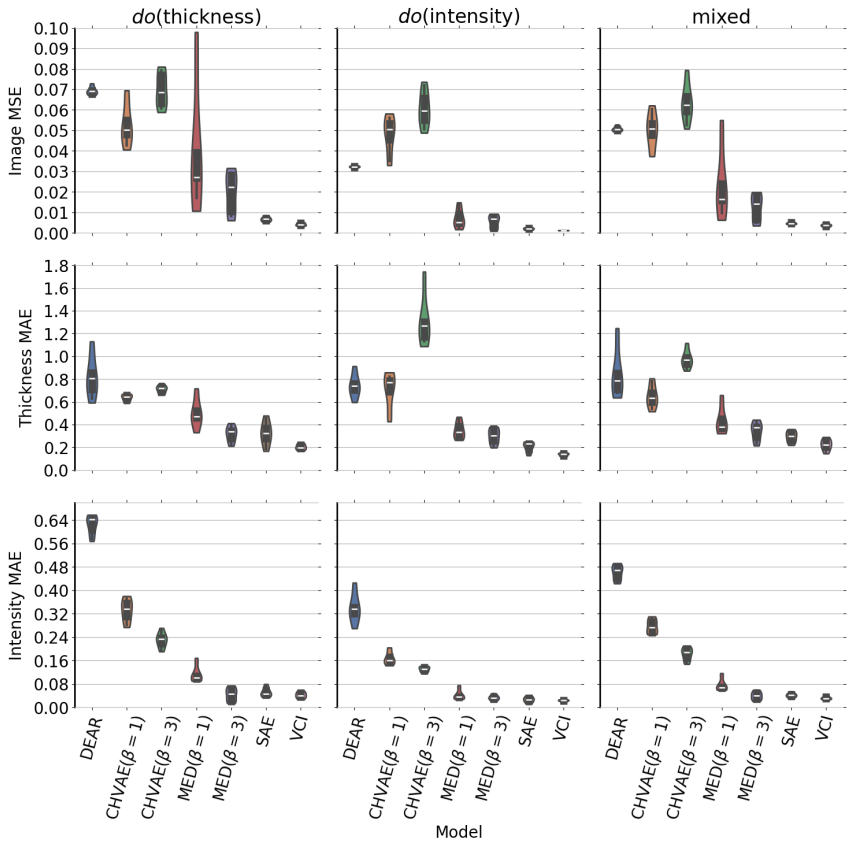

Figure 11: Violin plots of Image MSE, Thickness MAE and Intensity MAE on benchmark models and ours across five independent runs.

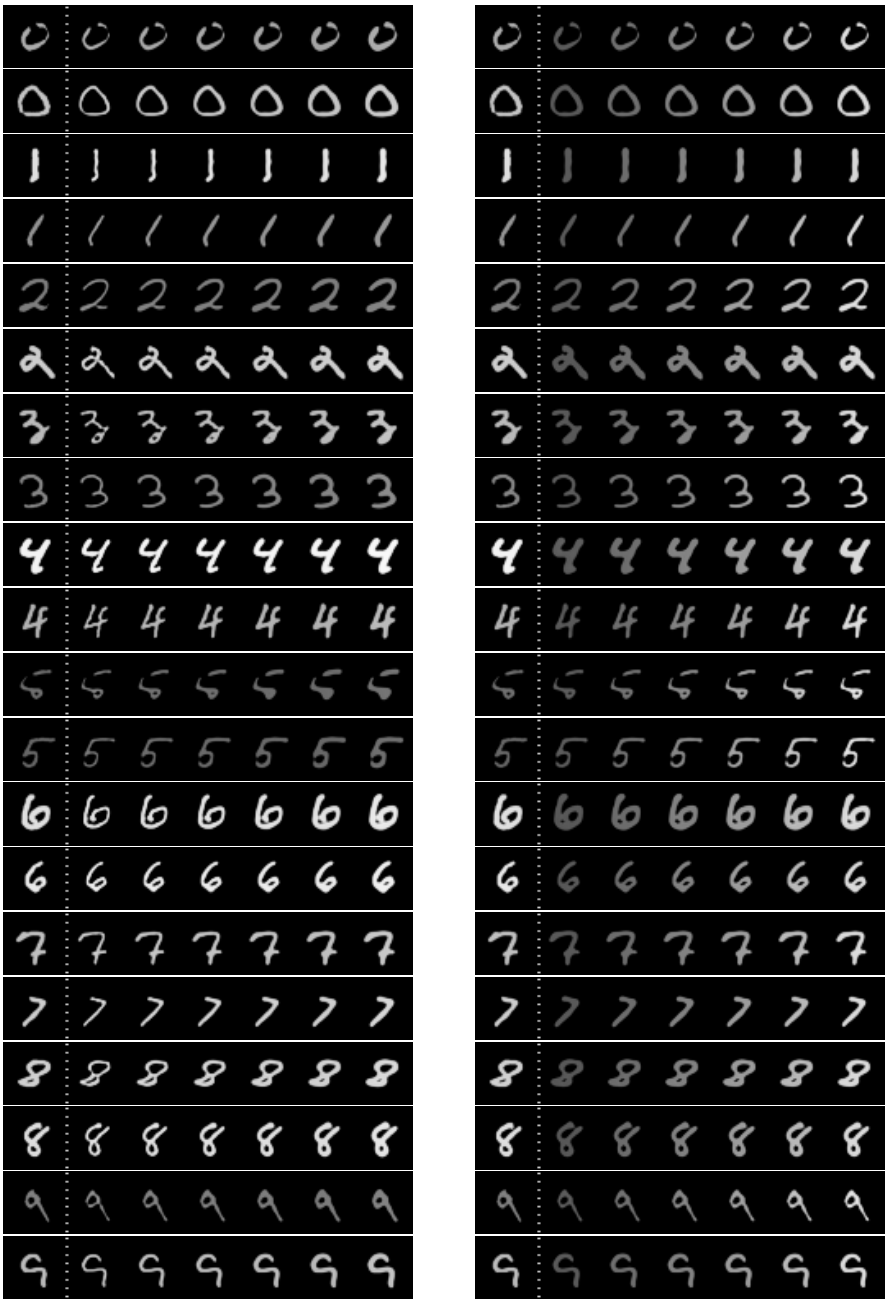

(a) *do*(thickness). (b) *do*(intensity).

Figure 12: Sampled results on the test set of Morpho-MNIST. The left most image of each set is the original image. These results are non-cherry-picked in terms of model performance (picking was conducted to make sure there is a variety of digits and styles, but not based on performance).

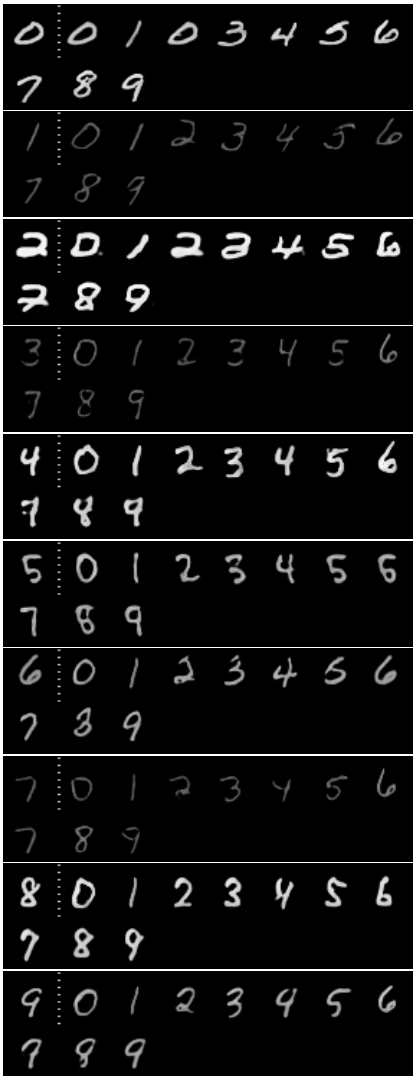

Figure 13: Sampled results on the test set of Morpho-MNIST on digit intervention. Note that these results do not have quantifiable counterfactual truths which we can evaluate on the capacity of intervening thickness and intensity in Table 2.